UNIVERSITY OF CALIFORNIA

Santa Barbara

# The Role of Redox Chemistry in Mussel Byssus

A dissertation submitted in partial satisfaction of the

requirements for the degree Doctor of Philosophy

in Biochemistry and Molecular Biology

by

Eric Valois

Committee in charge:

Professor J. Herbert Waite, Chair

Professor Alison Butler

Professor Denis Clegg

Professor Max Wilson

March 2020

The dissertation of Eric Valois is approved.

_____

Dr. Alison Butler

_____

Dr. Denis Clegg

_____

Dr. Max Wilson

_____

Dr. J. Herbert Waite, Committee Chair

December 2019

[This page is optional]

The Role of Redox Chemistry in Mussel Byssus



by

Eric Valois

“When you have eliminated all which is impossible, then whatever remains, however improbable, must be the truth.”

-Sherlock Holmes

## ACKNOWLEDGEMENTS

The pursuit of my Ph.D. began in 2013 as a master's student. It was during that time I arrived in Dr. Waite's Protein Physical Biochemistry and promptly received 3 points of a possible 10 on the first homework assignment. From then on, I knew I was in for a challenging yet rewarding adventure. Despite my early struggles, Herb never lost sight of my potential. Now, 6 years along, under Herb's guidance I have become a competent scientist who appreciates the virtues of basic sciences and knows that nature will always have more to teach us. I want to thank Herb for his unwavering support despite all of my 'distractions'. Being an advisor is no easy task. An advisor must walk the fine line between intervention and letting their students fail; no one is better at this than Herb. As a result, Herb's students gain a complete knowledge of the scientific process from question asking to experimental design to data interpretation. Most importantly, as Herb always says, "Its more important to be a diver than a surfer". A reference to the fact that transformative science involves asking deep questions that most overlook in favor of the superficial.

I also want to thank William Wonderly and Dr. Daniel DeMartini. The success of any Ph.D. student is largely dependent upon those around them. These two share my successful completion of this degree. Primarily due to their willingness to always talk about science, no matter how outlandish the idea may have been. I could also always count on them for a mental break, whether it was an unnecessary walk to the UCen or hunting for mushrooms and worms.

I want to thank my parents, Diane and Gerry for their unwavering support. My journey to a Ph.D. was certainly not a linear path. It began at Cuesta, then moved to UC Davis which

was accompanied with a major change from biology to nutrition and then a second change to Neuroscience. When I said I wanted to go to Santa Barbara, with no real plan, they supported me in my venture, always claiming they knew I would land on my feet. Despite more than a decade of schooling, they continue to encourage my endeavors.

Lastly, I want to thank Dr. Jacklyn Valois. When our journey began together, we were merely two college students bumbling round the world void of any degrees. From our early beginnings at Davis, we have grown and matured together, enduring extremely difficult times during each of our pursuits for doctorate degrees. You have always pushed me to pursue my dreams, often times at the sacrifice of your own happiness, and for that I will never be able to repay you. It is with your love and support that I have been able work my way through one of my life's most difficult tasks. Our path toward my completion of this dissertation, while not always parallel, has gone something like this. Just two college kids who met in the most unlikely of ways, to college graduates living together, to two people independently pursuing doctorates, and finally, to engagement and marriage. And at the end of it all, we are two Doctors, maturing together in a pursuit to make the world a better place. Thank you for all that you have done for me over the years.

Curriculum Vitae of Eric Valois
October 2019

## Education:

**Ph.D. Biomolecular Science and Engineering**, 2019
University of California at Santa Barbara,

**B.S. Neurology, Physiology and Behavior**, 2012
University of California at Davis,

## Research Experience:

**Waite Lab, UC Santa Barbara** 2013 – 2019
*Ph.D. Candidate*

- Design and execution of experiments characterizing the redox chemistry of the mussel byssus as well as characterization of biochemical and mechanical properties of proteinaceous load bearing biomaterials.
- Proposal writing for funding sources and synchrotron access.

**Genentech, Inc.** 2014
*Graduate Student Intern*

- Member of Research and Early Development Team (gRED) in their Protein Sciences Division
- Design and manufacture of multifunctional antibodies to be used in the treatment of macular degeneration.

**M.I.N.D. Institute** 2010
*Undergraduate Researcher*

- Member of the Noctor Lab, our research focused on the neurodegenerative disease Fragile-X
- Duties involved preparation of embryonic mice brain tissue for histological and immunohistochemical staining.

## Publications:

**Valois E**, Hoffman C, Demartini DG, Waite H. The Thiol-Rich Interlayer in the Shell/Core Architecture of Mussel Byssal Threads. Langmuir. 2019. DOI: 10.1021/acs.langmuir.9b01844

Degen G, Lewis R, Andersen-Eguiluz R, **Valois E**, Butler A. Impact of Molecular Architecture and Adsorption Density on Adhesion of Mussel-Inspired Surface Primers with Catechol-Cation Synergy. J. Am. Chem. Soc. 2019. DOI: 10.1021/jacs.9b04337

Mukherjee S, Xie R, Reynolds V.G., Uchiyama T, Levi A.E., **Valois E**, Wang H, Chabinyc M, Bates C.M., *Universal Approach to Photo-Crosslink Bottlebrush Polymers.* Macromolecules. **Accepted, Dec 2019**

**Valois E,** Mirshafian R, Waite H. *Phase-Separated Redox Batteries in Mussel Adhesion*. Science Advances. 2019. **In Revisions, Sept 2019.**

Wonderly W, Demartini D, Phan T, **Valois E,** Helgeson J, Waite J.H *Catalyst, template, and copolymer in film formation: A multitasking polypeptide from bloodworm jaws.*. In preparation

**Presentations:**

E. Valois (2019) Phase-separated Redox Reservoirs in Mussel Adhesion. Presented at Adhesion '19, Bristol, United Kingdom.

E. Valois. (2018) Cysteine Rich Mechanical Interphase of the Mussel Byssus Thread. Presented at the Gordon Research Conference on Biomimetic Materials, Les Diablerets, Switzerland.

E. Valois. (2017) Cysteine Rich Mechanical Buffer of the Mussel Byssus Thread. Presented at the Gordon Research Conference on Biological Interfaces, Hong Kong, China.

E. Valois (2014) PEGylating Anti-fD: Foreseeing the Future in the Treatment of Geographic Atrophy. Presented at Genentech's Interns Day. San Francisco, USA.

**Teaching Experience**:

| | | |
|---|---|---|
| **Instructor of Record** | Biochemistry | S, F 2016 |
| **Teaching Assistant** | Protein Processing | S, 2016 |
| **Teaching Assistant** | Protein Physical Biochemistry | W 2016 |
| **Teaching Assistant** | Biochemistry | S, F, 2015 |
| **Teaching Assistant** | Oncogenesis | S, 2015 |
| **Teaching Assistant** | Introductory Biology Lab | F, 2013, 2014,2015 |

ABSTRACT

The Role of Redox Chemistry in Mussel Byssus

By

Eric Valois

The mussel byssus is a collection of extra-organismal, acellular, proteinaceous load bearing structures that are radial displayed and utilized by marine mussels to secure themselves to a multitude of substrates. A single byssal thread can be subdivided into the loading bearing thread and adhesive plaque, which provide tensile strength and adhesive strength respectively. Both regions of the byssus face their own unique challenges and have devised independent mechanisms to protect themselves against oxidative stresses. Here we present evidence the mussel utilizes isolated redox compartments to protect 3, 4-dihydroxyphenylalanine (Dopa) from oxidative damage in both the thread and plaque, permitting long lasting mechanical performance of the byssus.

The byssus thread is an extremely tough core-shelled fiber that dissipates substantial amounts of energy during tensile loading. The mechanical performance of the shell is critically reliant on Dopa's ability to form reversible iron-catecholate complexes at pH 8. However, the formation of these coordinate crosslinks is undercut by Dopa's oxidation to Dopa-quinone, a spontaneous process at seawater conditions. Using a combination of

electron and atomic force microscopy we identify a previously undescribed stratum situated between the core and shell. Spectroscopy results indicate this region is rich in thiol and thus will be called the thiol rich layer (TRL). We propose the TRL acts as an electron sink to protect the shell against oxidation. Additionally, indentation type atomic force microscopy reveals the TRL has intermediate mechanical properties which act as a mechanical buffer between the shell and core.

The adhesive plaque is also reliant on Dopa. Dopa in the plaque is primarily responsible for strong adhesion but only if protected from oxidation at the adhesive-substratum interface. Dopa oxidation is thermodynamically favorable in seawater yet barely detectable in mature plaques. Experiments were designed to understand how plaques insulate Dopa-containing mfps against oxidation. Spectrometry and confocal fluorescence results indicate seawater sulfate triggers a mfp3 and mfp6 liquid-liquid phase separation (LLPS). Subsequently, cyclic voltammetry of LLPS material demonstrates DOPA's redox potential is phase dependent. Furthermore, mass spectrometry and redox exchange assays indicate Dopa-containing mfp-3 and mfp-6 in phase-separated droplets remain stable despite rapid oxidation in the equilibrium solution. Taken together, the results suggest that a cohort of oxidation-prone proteins is endowed with phase-dependent redox stability. Moreover, in forming LLPS compartments, Dopa-proteins become reservoirs of chemical energy which can be called upon in the event of oxidative damage.

TABLE OF CONTENTS

LIST OF FIGURES

# Chapter I

# Background

## ***Mytilus californianus***

From an evolutionary perspective, *Mytilu*s is notable for its adaptive emergence from the benthos where many other bivalve varieties still reside [1]. The origins of *Mytilus* can be traced to the Northwest Pacific Ocean where *Mytilus californianus, Mytilus edulis, Mytilus galloprovincialis* and Mytilus trossulus shared a common ancestor ~7.6 million years ago[2]. While the later three comprise the 'blue mussel' species complex, sharing a common ancestor as recently as 3.5 million years ago, *Mytilus californianus* represents a distinct evolutionary lineage that can be found in an expansive geographical range in the northern Pacific arcing from Alaska to Baja[2].

*Mytilus californianus (M.cali)*, also known as the California sea mussel, is a sessile marine mussel that is the most abundant bivalve found in the intertidal zones of the California coast [2]. Its shell can be distinguished from other mytilids by the presence of protruding radiating ridges[3] and the presence of its umbo at the extreme anterior end [3] . M. cali can reach lengths up to 250mm in length and live up to 50 years [4].

## The Mussel Byssus:

Emergence into the littoral habitat is complicated by waves crashing at 20m/s, predation, cyclic dehydration and other environmental stresses [5], yet the mussel spends the majority of its life securely anchored to an intertidal substrate[1]. In order to achieve this remarkable feat, the marine mussel has devised a holdfast called the byssus. The word byssus or βύσσος which means flax linen [1,6] in Greek originates from a mistranslation by Theodorus Gaza of Aristotle's description of *Pinna* in his "History of Animals" in which Aristotle actually states that *Pinna* is secured to the bottom or βυσσός (as in abyss bottomless). The byssus is a collection of radially displayed threads with adhesive plaques and is comprised of three distinct regions; stem, thread and plaque. While the thread itself can be subdivided into the proximal and distal region, only the distal portion will be discussed henceforth.

## Ultrastructure of the thread-plaque system

### Core:

Byssus threads, which tether the mussel to its substrate, are 2-5cm in length and 100-200 um in diameter [7]. The principal component of the thread, comprising 96% by dry weight, are extensible collagen-like proteins called preCols [7-9]. preCols possess a triple helical core flanked on either side by highly extensible domains with semblance to silk [8,9]. preCol triple helical monomers are high aspect ratio proteins (1.5nm in width 200 nm in length), which assemble into hexagonal 6+1 bundles ~8.5 nm in width [10-12]. These 6+1 bundles serve as the 'building block' of the thread, further assembling into fibers. Whilst sharing many similarities with mammalian collagens, mussel collagen fibers lack the classical 67 nm banding pattern visible by transmission electron microscopy (TEM) and

atomic force microscopy (AFM) [8]. Despite the lack of visible banding, small angle X-ray scattering shows semi-crystallinity between bundles with an axial spacing of 13.2 nm and bundle center to center distance of 20.4 nm [10,13].

**Cuticle:**

The core is ensheathed by a thiol rich layer (TRL) discussed in a later chapter. Enveloping the core and sheath, and in direct contact with the external environment, is a 2-5 um layer known as the cuticle [14]. The cuticle, who's major protein component is mfp-1[15], is a granular composite material. Granules contained in the cuticle of *M. cali* are approximately 200 nm in diameter and are regularly distributed throughout [14]. Surrounding the granules is a homogenous matrix resulting in a 1:1 volume fraction ratio of matrix to granules [16].

**Plaque:**

Continuous with the distal end of the thread is the adhesive plaque. Macroscopically, the plaque made by adult mussels is an ellipsoid disc approximately 3mm wide by 5 mm long [17]. At the periphery, the plaque thins to >50um, forming an almost smooth continuum with the substrate [17]. Cross-sections of the plaque reveal the three distinct phases. First, a fibrous extension of the distal thread exists at the center of the plaque. In this region, collagen fibers penetrate the plaque, reaching to within 3 $\mu$m of the substrate [17]. Second, the bulk of the plaque is a homogenous material of interconnected trabeculae, or foam. Two characteristic length scales comprise the foam; a dense meshwork with ~100nm struts interpenetrated by pores larger than 1 $\mu$m [18]. Third, the adhesive surface is a contiguous dense film.

## Mechanics of the thread-plaque system

### Thread:

A mussel's survival is dependent upon its ability to withstand displacement by waves that exert hydrodynamic forces in excess of 10N [19]. The mussel byssus has evolved over 300 million years with the sole purpose of firmly securing the mussel to solid supports in its habitat. Under tensile loading, the distal thread behaves like a typical elastomer with three unique phases: 1) initial elastic regime, 2) yield followed by zero stiffness extension, and 3) post-yield stiffening prior to failure [20].

The elastic regime of a tensile stress-strain curve exists at low strains (>10%). Within this regime, the thread has a measured modulus of approximately 850 MPa [20-22]. Furthermore, and perhaps more importantly, at low strains the distal thread shows exceptional resilience (up to 90%), with cyclic loads being indistinguishable from the pervious. Resilience is a measure of elastic efficiency and should be 100% for perfectly elastic materials[22].

When strain is increased beyond 20% the thread yields [21], transitioning from elastic to plastic deformation. The post yield phase is characterized by zero force extension, i.e. 0 MPa stiffness, from 20-40% strain. In this regime, the material experiences molecular re-orientation (Vincent), which is evident by X-ray scattering [9]. In these experiments, as threads are strained from 0 to 45%, a shift from high to low q-space is observable, representing an increase in real-space of the flanking domains. While elastically deformed threads exhibit high resilience, plastically deformed threads are only ~30% resilient, with a majority of the potential energy being dissipated as molecular friction [21]. The ability to undergo reversible yield, thought to be the most important mechanical attribute of the

mussel byssus[20], serves three critical roles in byssus performance. First, it increases the toughness of individual threads by preventing brittle fracture. Second, it permits reorientation of the thread parallel to the direction of the applied load [20]. Third, it promotes engagement of additional threads. Consequently, the load is distributed over a larger cross-sectional area, effectively reducing the stress experienced by any individual thread [20-22].

At strains exceeding the critical yield strain the byssal thread experiences stress softening. Stress softening, known as the Mullin's effect, is common in many materials and is typically the result of irreversible bond breakage [23]. When the distal thread is repetitively cycled to strains beyond yield, each cycle becomes less stiff than the previous [21]. However, contrary to typical materials, the distal thread is capable of time dependent recovery of initial stiffness in a process termed 'self-healing' [9,21]. When left unstressed, 50-60% of initial stiffness is recovered after only 30 min, though 100% recovery takes more than 24hours [7,9,21]. Exceptionally, byssus self-healing occurs without extrinsic inputs, namely cellular aid [9]. Given the predominantly proteinaceous composition, self-healing can be attributed to reversible structural and biochemical contributions only.

**Plaque:**

As described by Bell et al., the byssus as a whole can be thought of as a series of chain links [20] starting with the stem and terminating at the plaque. As the saying goes, a chain is only as strong as its weakest link: for the byssus, that link is the adhesive plaque [20]. Three modes of plaque failure are easily observable; adhesive failure, cohesive failure and plaque-thread junction failure [19,24]. For plaques pulled at 45 degrees (from horizontal), adhesive failure is most commonly observed [19]. Plaques pulled in this way experience strains below the detectable limit at the periphery [19]. However, strains at thread plaque-

junction exceeded 100% [19]. In mushroom shaped structures, much like the mussel plaque-thread, when the distance from the axis of the fiber (q) is larger than the radius of the fiber (r) such that q/r>1, the stress field at the edges is slightly compressive. Subsequently, slight defects in the compressive region of adhesive contact will not propagate [25]. Conversely, stress states are concentrated in regions were q/r<1, resulting in high stress/strain near the fiber stalk which ultimately lead to adhesive failure propagation from the center outward [19].

Decreasing the pull angle to 20 degrees (from horizontal) results in the largest forces necessary to initiate adhesive failure. As a result, the frequency at which adhesive failure is observed decreases but cohesive failure increases. According to Kendall's approximation for peeling of adhesive of thin films, adhesion energy scales linearly scales with $1/(1-\cos(\theta))$ [26], with $\theta$ denoting the pull angle with respect to normal. Thus, small peel angles produce the largest adhesion energies.

While both Kendall et al. and Desmond et al. argue adhesion strength and failure mode are largely geometry dependent, Burkett et al. recognized that surface chemistry may alter failure mode independent of geometry. Plaques adhered to low surface energy substrates, such as polyvinyl chloride (PVC), failed adhesively ~98% of the time. Conversely, plaques adhered to high surface energy substrates, such as glass, failed at the plaque thread junction ~91% of the time [24].

The energy required to remove a single plaque from the surface is approximately 95 J/m^2 yet the plaque's most adhesive protein, mfp-5, has an adhesion energy 5 orders or magnitude less at ~14 mJ/m^2. This dramatic discrepancy indicates the supramolecular structure of the plaque is capable of dissipating tremendous amounts of energy.

Furthermore, it reveals there is an important synergy between geometry and surface chemistry, which will be discussed in the section pertaining to biochemistry of the plaque.

## Biochemistry

The unique mechanical properties of byssus derive from its composite architecture at multiple length scales. In this section I will discuss the biochemistry of these structures.

### Core:

The core of the thread is composed of collagen like molecules whose block composition from N- to C- terminus includes a histidine rich domain, variable flank domain A, central collagen domain, an acidic patch, variable flank domain B and a second histidine rich domain[12]. The central collagen domain comprises between ~50-60% of the total preCol sequence and maintains a typical G-X-Y collagen motif capable of forming a triple PPII-type helix [27].

It is known that when Proline (Pro,P) and Hydroxyproline (HPro) occupy positions X and Y the helix is thermodynamically stable and that any aberrations are destabilizing [28]. M cali contains three destabilizing deviations from the canonical sequence. [28]. Two of these changes are Gly deletions, similar to those observed in M gallo. and M edulis, however, the third is not seen in any other species. This novel change is the introduction of a four amino acid insert, Val-Val-Gly-Gly [28]. These changes in Gly-X-Y typically result in kinks in the rod structure [29,30], yet what mechanical advantage these kinks provide is still a mystery[28].

Flanking the central collagen domain on both the N- and C- termini are the variable domains. Specific to preCol-D, there are 7 poly-alanine runs between 11 and 14 residues in

length which resemble dragline silks found in spiders[27,29,31,32]. Poly-alanine runs are known to create stacks of beta-pleated sheets which contribute to the thread's material stiffness by increasing its degree of crystallinity [29,33]. By combining FTIR with in-situ tensile testing, Hagenau et al. were able to demonstrate at low stresses that the 966 $cm^{-1}$ wavenumbers, corresponding to beta sheets, shifted to lower frequencies. At high stresses, this band shifted to higher frequency but its angle-dependent intensity remained constant. Taken together, these data indicate the silk domains are load bearing and highly oriented but at some critical stress become non-oriented and thus lose their ability to bear load [33]. Additionally, the silk-like domains contain Gly-Gly-X and Gly-X-Gly-X domains capable of forming $3_1$ helixes and beta-sheet structures [33].

Beyond the variable domains at both termini are Histidine rich domains. Here, histidine accounts for 20 mol% of all residues and is often found in tandem with Ala or Gly [32]. For example, the N-terminal region contains 4 tandem repeats of tetrapeptide HAHA [32]. Given that the collagen domain is liberated intact by pepsin treatment of byssus and the silk domain is incapable of forming covalent cross links, the His-rich domain could serve as the only point of cross linking in the preCols [34]. Two types of cross-links could be readily formed by the histidine domains. First are the intermolecular bis- and tris-histidinyl metal complexes similar to those found in metalloproteases and carbonic anhydrase [32]. The second are the result of a Michael addition of histidine or lysine to DOPAquinone [35].

The unique block architecture and amino acid composition of the preCols result in a triple helical tropocollagen-like unit with a bent collagenous core. These units further assemble in to 6+1 bundles that resemble a 'banana' or 'flower' [12]. Prior to assembly into a mature thread, these bundles are stored in ellipsoidal secretory vesicles in the mussel foot.

Bundles within the granules self-assemble into smectic liquid crystals (LC) [36]. In lyotropic LCs, once the concentration of mesogen surpasses a critical concentration, it is energetically more favorable for high aspect ratio molecules to align anisotropically [37]. During thread processing, higher order organization of the mesophase reduces the bulk viscosity, resulting in a more aligned, stronger product [37]. Once called upon to make a new thread, vesicles are secreted into a groove running the length of the mussel foot and rapidly self-assemble under seawater conditions [38].

## Cuticle

As previously mentioned, the cuticle plays a critical role in protecting the core against damage and despite all that is known about its mechanical function, little is known about the biochemistry. To date, only a single protein, mussel foot protein 1 (mfp-1), has been associated with the M cali byssal cuticles [39]. Mfp-1 is a large protein (MW ~ 110 kDa) comprised of 85 tandemly repeated decapeptides of consensus sequence AKPSY*O*OTY*K [40,41], where O* denotes dihydroxyproline, O is hydroxyproline and Y* is DOPA, a catecholic amino acid derived from post translational hydroxylation of tyrosine. Mfp-1 is characterized by an isoelectric point>10 and a predominant lack of secondary structure [42]. However, its most striking characteristic is the presence of ~15 mol% DOPA. Included alongside mfp-1 is an inorganic component made principally of metal ions, namely iron and calcium [42]. Although calcium comprises approximately 90% of the inorganic content, mineralization is surprisingly absent from the cuticle and most studies to date have focused on the role of iron [43] [42,44].

There are many examples in nature where catechols and iron interact to form catecholate-iron(III) complexes, ranging from small molecule bacterial siderophores to iron core enzymes that utilize catechols as their substrates [44]. Titrations of purified mfp-1 with ferric iron resulted in a purple colored solution with an absorption maximum of 500 nm [44], indicating mfp-1's ability to form tris(catecholate) complexes *in vitro* [44]. Given the colocalization of dopa and iron in the cuticle, formation of Dopa-iron complexes seemed inevitable, yet *in vivo* evidence was lacking until 2010. Using confocal Raman spectroscopy, Harrington et al. successfully showed peaks corresponding to bidentate interactions of catecholic oxygen with ferric iron (550 $nm^{-1}$, 596 $nm^{-1}$ and 617 $nm^{-1}$) were exclusively localized in the cuticle. Conversely, the aliphatic C-H stretch was homogenously distributed throughout the thread [42]. Additionally, studies conducted on *M. gallo* indicated the such complexes are not evenly distributed within the cuticle; instead, the metal chelate complexes are concentrated within the granules [42]. The high log stability constant, ~10, implies these complexes are serving as effective crosslinks between Dopa residues, thus increasing the cohesive capabilities of mfp-1 [34]. Furthermore, it has been proposed that the complexes are hygroscopic thus preventing the cuticle from becoming brittle as a result of dehydration [45].

The final stage of thread formation is cuticle secretion over top of the previously formed core. However, unlike the proteins in the core, mfp-1 lacks secondary structure necessary for liquid crystal formation, forcing the mussel exploit other approaches for cuticle deposition. Instead the mussel utilizes coacervation. Complex coacervation was first described by Bungenberg de Jong in 1949 as a fluid-fluid separation that occurs upon mixing two oppositely charged electrolytes resulting in a charge neutral complex. Simple coacervates, occur when a single polyelectrolyte is capable of self-neutralization through

modulation of ionic strength, pH and polyelectrolyte concentration. Sheer-thinning viscous properties and low interfacial tension allow coacervates to easily be secreted through an intricate duct system and rapidly coat surfaces, making it an ideal mechanism for cuticle delivery [46]. Many factors contribute to this phenomenon such as charge density, hydrophobicity, polymer weight, ionic strength, temperature, etc. Mfp-1 is capable of both complex and simple coacervation as demonstrated by Miller et al. and Kim et al. Studies with hyaluronic acid and mfp-1 demonstrate the ability to form complex coacervates via charge neutralization [47]. It is currently hypothesized that *in vivo* mfp-1 may complex with an anionic $Ca^{2+}$ binding protein, yet direct evidence is lacking [47]. Simple coacervation of recombinant mfp-1 (rmfp-1) can be induced by increasing the ionic strength of the solution to ~0.7M [48]. Typically, high ionic strength solutions disrupt the coacervate phase by screening electrostatic interactions between oppositely charge poly-electrolytes [48-50]. However, in the mussel system, high ionic strength reduces electrostatic repulsions that arise from the predominant cationic nature of mfp-1 [48]. Subsequently, allowing for cation-$\pi$ interactions to drive and stabilize the coacervate [48].

**Plaque:**

At the plaque-substrate interface exists a complex assortment of mussel foot proteins, namely -2, -3, -4, -5 and -6 that are responsible for long term adhesion[51]. For purposes of this dissertation, I will focus the discussion on mfps -3, -5 and -6.

Mfp-3 and mfp-5 are considered to be priming proteins found at the adhesive interface. The mfp-3 family contains more then 30 variants divided into 2 families known as ‘Fast’ and ‘Slow’. The fast variants contain more positive charges than slow family and

were aptly named for the speed at which they traveled in an acid-urea PAGE experiment [52]. While mfp-3 variants are abundant, mfp-5 exists as phosphorylated and unphosphorylated forms [53]. Furthermore, both proteins are characterized by high isoelectric points, and high DOPA mol%, causing them to be highly adhesive and susceptible to oxidative damage.

Experiments conducted using the surface forces apparatus (SFA) revealed that at pH 2.5, the adhesion energy of mfp-5 to mica is ~15 $mJm^{-2}$, exceeding the interaction energy of the biotin-streptavidin complex [51,53,54]. Mica, an inorganic aluminum silicate with surface chemistry reminiscent of rocks found in a mussel's natural habitat, possesses an alumina/silica oxide surface spacing of 0.28 nm, closely matching that of the hydroxyl spacing in DOPA [55]. Thus suggesting, at low pH (~2.5) the predominant interaction between dopa containing mfp's and mica is bidentate hydrogen bonding [51,55]. These highly oriented bi-dentate hydrogen bonds produce a bond lifetime that is 6 orders of magnitude longer than that of a single hydrogen bond, ensuring that once adsorbed, protein desorption is unlikely [51]. Adsorbed DOPA experiences a binding mode transition as a function of pH. As pH is titrated upwards, a DOPA residue in contact with a metal oxide surface will transition from bidentate hydrogen bonds, to a combination of one H-bond with one coordinate bond, to bidentate binuclear coordinate bonds [51,56]. Additionally, interactions between mfp-5's phosphate groups and $Cat^{2+}$ become more stable[51].

Despite the large adhesion energies once adsorbed, adhesion can be foiled by the presence of surface bound water, which competes with DOPA for hydrogen bonding sites at the surface. Hydrated cations bound to the substrate surface create a hydration layer hindering protein adsorption and subsequent H-bonding [57,58]. To mitigate this issue, the mussel has placed lysine in close proximity to the catecholic residues. Lysine has the ability

to evict hydrated surface bound cations, subsequently reducing the hydration layer [57] and paving the way for long lived bidentate hydrogen bond formation.

Deposition can be further enhanced by involving liquid-liquid phase separation such as coacervation. Plaque proteins are injected into the acidified distal depression as solutes [59], and undergo a phase transition upon exposure to seawater conditions[60]. *In vitro*, mfp-3 coacervate deposition resulted in four times more material binding to the surface compared with the solution state [61], as well as decreased desorption upon rinsing. Additionally, ATR-FTIR indicates increased dehydration of the substrate surface especially when using Dopa-containing proteins [61].

Although equilibration toward seawater conditions may be beneficial for deposition it is detrimental to adhesion. For instance, Mfp-5 adhesion diminishes 75% at pH 5.5 and is effectively abolished at pH 7.5 [54,62]. Simply lowering the pH was insufficient at restoring adhesion [63]. Losses in adhesion were attributed to oxygen dependent oxidation of DOPA to DOPAquinone, which is not capable of the metal coordination and H-bond formation essential for stable bonding [54,62,64,65]. Subsequent SFA tests combining mfp-3 at acidic pH with the strong oxidizer periodate produced nominal adhesion, thus confirming the correlation between quinone formation and adhesion loss [63].

Seawater contains large amounts of dissolved oxygen and high trace metal content resulting in a standard redox potential of approximately 600 mV, substantially higher than that of DOPA [51,66]. As a result, DOPA oxidation via oxygen reduction is a likely process, however DOPA remains detectable for upwards of 1 month in mature plaques [67]. To combat oxidation and oxidative losses, the mussel incorporates reducing compartments and antioxidant proteins, chiefly mfp-6 [64].

Mfp-6 is a 11.5kDa protein with a composition that is ~11 mol% cysteine giving rise to a reducing capacity of 17 $e^-$ per protein [64,68]. When introduced to oxidized mfp-3 films, mfp-6 was able to fully restore adhesion [63]. Interestingly, reducing activity of mfp-6 persists at pHs as low as 3, suggesting some of mfp-6's thiols possess $pK_a$'s well below the typical 8-9 [63]. The rescue process requires two subsequent nucleophilic attacks initiated by a cysteinyl thiolate. First, a thiolate anion adds to carbon 5 in a Michael addition reaction, followed by attack of the thioether by a second thiolate resulting in a restored DOPA and cystine [69,70]. The question of mfp-6's ability to maintain DOPA is certainly one of stoichiometry. As the number of reducing thiols is consumed, a buildup of 5-S-cysteinylDOPA occurs [68]. To date, redox poise has been somewhat of a mystery. How do thiols persist for extended periods of time? How does the mussel protect both thiols and DOPA from immediate oxidation despite existing in highly oxidizing seawater? These questions will be addressed in Chapter 3.

**References:**


1. Yonge CM. On The Primitive Significance of the Byssus in the Bivalvia and its Effects in Evolution. *https://doiorg/101017/S0025315400004495*. December 2008:1-13. doi:10.1017/S0025315400004495.

2. Lockwood BL, Connor KM, Gracey AY. The environmentally tuned transcriptomes of Mytilus mussels. *J Exp Biol*. 2015;218(Pt 12):1822-1833. doi:10.1242/jeb.118190.

3. Jones TL, Richman JR. On Mussels: Mytilus Californianusas a Prehistoric Resource. *North American Archaeologist*. 1995;16(1):33-58. doi:10.2190/G5TT-YFHP-JE6A-P2TX.

4. Shaw WN. Species Profiles: Life Histories and Environmental Requirement of Coastal Fishes and Invertebrates (Pacific Southwest): California Sea Mussel and Bay Mussel. *Biological Report Fish and Wildlife Servies*. 1988:1-24.

5. Carrington E. Drag and dislodgment of an intertidal macroalga: consequences of morphological variation in Mastocarpus papillatus Kutzing. *Journal of Experimental Marine Biology and Ecology*. 1990;139:185-200.

6. Waite JH. Adhesion a la Moule. *Integrative and Comparative Biology*. 2002;42(6):1172-1180. doi:10.1093/icb/42.6.1172.

7. Harrington MJ, Gupta HS, Fratzl P, Waite JH. Collagen insulated from tensile damage by domains that unfold reversibly: in situ X-ray investigation of mechanical yield and damage repair in the mussel byssus. *Journal of Structural Biology*. 2009;167(1):47-54. doi:10.1016/j.jsb.2009.03.001.

8. Qin X, Waite JH. Exotic collagen gradients in the byssus of the mussel Mytilus edulis. *Journal of Experimental Biology*. 1995;198(Pt 3):633-644.

9. Krauss S, Metzger TH, Fratzl P, Harrington MJ. Self-Repair of a Biological Fiber Guided by an Ordered Elastic Framework. *Biomacromolecules*. 2013;14(5):1520-1528. doi:10.1021/bm4001712.

10. Krauss S, Metzger TH, Fratzl P, Harrington MJ. Self-Repair of a Biological Fiber Guided by an Ordered Elastic Framework. *Biomacromolecules*. 2013;14(5):1520-1528. doi:10.1021/bm4001712.

11. Zucarrello-Vitellaro, L., 1980. The collagen gland of Mytilus galloprovincialis: an ultrastructural and cytochemical study on secretory granules. *Tissue & Cell or J. Ultrastruct. Res Elsevier*. 1980;73(2):135-147. doi:10.1016/S0022-5320(80)90119-7.

12. Hassenkam T, Gutsmann T, Hansma P, Sagert J, Waite JH. Giant Bent-Core Mesogens in the Thread Forming Process of Marine Mussels. *Biomacromolecules*. 2004;5(4):1351-1355. doi:10.1021/bm049899t.

13. Bairati A, research LZCAT, 1976. The ultrastructure of the byssal apparatus of Mytilus galloprovincialis. *Springer*. doi:10.1007/BF00227043.

14. Holten-Andersen N, Zhao H, Waite JH. Stiff Coatings on Compliant Biofibers: The Cuticle of Mytilus californianusByssal Threads †,‡. *Biochemistry*. 2009;48(12):2752-2759. doi:10.1021/bi900018m.

15. Holten-Andersen N, Slack N, Proceedings FZMO, 2004. Nano-mechanical investigation of the byssal cuticle, a protective coating of a bio-elastomer. *cambridgeorg*. doi:10.1557/PROC-841-R3.7/Y3.7.

16. Monnier CA, DeMartini DG, Waite JH. Intertidal exposure favors the soft-studded armor of adaptive mussel coatings. *Nature Communications*. August 2018:1-9. doi:10.1038/s41467-018-05952-5.

17. Tamarin A, Lewis P, Askey J. The structure and formation of the byssus attachment plaque in Mytilus. *J Morphol*. 1976;149(2):199-221. doi:10.1002/jmor.1051490205.

18. Filippidi E, DeMartini DG, Malo de Molina P, et al. The microscopic network structure of mussel (*Mytilus*) adhesive plaques. *J R Soc Interface*. 2015;12(113):20150827–10. doi:10.1098/rsif.2015.0827.

19. Desmond KW, Zacchia NA, Waite JH, Valentine MT. Dynamics of mussel plaque detachment. *Soft Matter*. 2015;11(34):6832-6839. doi:10.1039/c5sm01072a.

20. Bell E, Gosline J. Mechanical design of mussel byssus: material yield enhances attachment strength. *Journal of Experimental Biology*. 1996;199(4):1005-1017.

21. Carrington E, Gosline JM. Mechanical design of mussell byssus: Load cycle and strain rate dependence. 2004.

22. Gosline J, Lillie M, Carrington E, Guerette P, Ortlepp C, Savage K. Elastic proteins: biological roles and mechanical properties. Bailey AJ, Macmillan J, Shrewry PR, Tatham AS, eds. *Philosophical Transactions of the Royal Society of London B: Biological Sciences*. 2002;357(1418):121-132. doi:10.1098/rstb.2001.1022.

23. Bueche F. Molecular basis for the mullins effect. *Journal of Applied Polymer Science*. 1960;4(10):107-114. doi:10.1002/app.1960.070041017.

24. Burkett JR, Wojtas JL, Cloud JL, Wilker JJ. A Method for Measuring the Adhesion Strength of Marine Mussels. *The Journal of Adhesion*. 2009;85(9):601-615. doi:10.1080/00218460902996903.

25. Spuskanyuk AV, McMeeking RM, Deshpande VS, Arzt E. The effect of shape on the adhesion of fibrillar surfaces. *Acta Biomaterialia*. 2008;4(6):1669-1676. doi:10.1016/j.actbio.2008.05.026.

26. Kendall K. The adhesion and surface energy of elastic solids. *J Phys D: Appl Phys*. 2002;4(8):1186-1195. doi:10.1088/0022-3727/4/8/320.

27. Waite JH, Vaccaro E, Sun C, Lucas JM. Elastomeric gradients: a hedge against stress concentration in marine holdfasts? *Philosophical Transactions of the Royal Society of London B: Biological Sciences*. 2002;357(1418):143-153. doi:10.1098/rstb.2001.1025.

28. Harrington MJ, Waite JH. Holdfast heroics: comparing the molecular and mechanical properties of *Mytilus californianus* byssal threads. *Journal of Experimental Biology*. 2007;210(24):4307-4318. doi:10.1242/jeb.009753.

29. Waite JH, Qin X-X, Coyne KJ. The peculiar collagens of mussel byssus. *Matrix Biol*. 1998;17(2):93-106. doi:10.1016/S0945-053X(98)90023-3.

30. Kilchherr E, Hofmann H, molecular WSJO, 1985. Structural model of the collagen-like region of C1q comprising the kink region and the fibre-like packing of the six triple helices. *Elsevier*. 1985;186(2):403-415. doi:10.1016/0022-2836(85)90114-7.

31. Hagenau A, Scheidt HA, Serpell L, Huster D, Scheibel T. Structural Analysis of Proteinaceous Components in Byssal Threads of the Mussel Mytilus galloprovincialis. Taubert A, ed. *Macromol Biosci*. 2009;9(2):162-168. doi:10.1002/mabi.200800271.

32. Qin X-X, Coyne KJ, Waite JH. Tough Tendons MUSSEL BYSSUS HAS COLLAGEN WITH SILK-LIKE DOMAINS. *Journal of Biological Chemistry*. 1997;272(51):32623-32627. doi:10.1074/jbc.272.51.32623.

33. Hagenau A, Papadopoulos P, Kremer F, Scheibel T. Mussel collagen molecules with silk-like domains as load-bearing elements in distal byssal threads. *Journal of Structural Biology*. 2011;175(3):339-347. doi:10.1016/j.jsb.2011.05.016.

34. Das S, Miller DR, Kaufman Y, et al. Tough Coating Proteins: Subtle Sequence Variation Modulates Cohesion. *Biomacromolecules*. 2015;16(3):1002-1008. doi:10.1021/bm501893y.

35. Xu REA. Characterization of Products from the Reactions of N-Acetyldopamine Quinone with N-Acetylhistidine. April 1996:1-9.

36. Priemel T, Degtyar E, Dean MN, Harrington MJ. Rapid self-assembly of complex biomolecular architectures during mussel byssus biofabrication. *Nature Communications*. 2017;8:1-12. doi:10.1038/ncomms14539.

37. Harrington MJ, Waite JH. pH-Dependent Locking of Giant Mesogens in Fibers Drawn from Mussel Byssal Collagens. *Biomacromolecules*. 2008;9(5):1480-1486. doi:10.1021/bm8000827.

38. Renner-Rao M, Clark M, ORCID: 0000-0003-1417-9251 MJH. Fiber Formation from Liquid Crystalline Collagen Vesicles Isolated from Mussels. *Langmuir*. August 2019:1-10. doi:10.1021/acs.langmuir.9b01932.

39. Lee BP, Messersmith PB, Israelachvili JN, Waite JH. Mussel-Inspired Adhesives and Coatings. *Annu Rev Mater Res*. 2011;41(1):99-132. doi:10.1146/annurev-matsci-062910-100429.

40. Sun C, Waite JH. Mapping chemical gradients within and along a fibrous structural tissue, mussel byssal threads. *Journal of Biological Chemistry*. 2005;280(47):39332-39336. doi:10.1074/jbc.M508674200.

41. Taylor SW, Chase DB, Emptage MH, Nelson MJ, Waite JH. Ferric Ion Complexes of a DOPA-Containing Adhesive Protein from Mytilus edulis. *Inorg Chem*. 1996;35(26):7572-7577. doi:10.1021/ic960514s.

42. Harrington MJ, Masic A, Holten-Andersen N, Waite JH, Fratzl P. Iron-Clad Fibers: A Metal-Based Biological Strategy for Hard Flexible Coatings. *Science*. 2010;328(5975):216-220. doi:10.1126/science.1181044.

43. Holten-Andersen N, Mates TE, Toprak MS, Stucky GD, Zok FW, Waite JH. Metals and the Integrity of a Biological Coating: The Cuticle of Mussel Byssus. *Langmuir*. 2009;25(6):3323-3326. doi:10.1021/la8027012.

44. Taylor SW, Chase DB, Emptage MH, Nelson MJ, Waite JH. Ferric ion complexes of a DOPA-containing adhesive protein from Mytilus edulis. *Inorg Chem*. 1996;35(26):7572-7577. doi:10.1021/ic960514s.

45. Monnier CA, DeMartini DG, Waite JH. Intertidal exposure favors the soft-studded armor of adaptive mussel coatings. *Nature Communications*. August 2018:1-9. doi:10.1038/s41467-018-05952-5.

46. Yang B, Jin S, Park Y, Jung YM, Cha HJ. Coacervation of Interfacial Adhesive Proteins for Initial Mussel Adhesion to a Wet Surface. *Small*. 2018;14(52):1803377–12. doi:10.1002/smll.201803377.

47. Miller DR, Das S, Huang K-Y, Han S, Israelachvili JN, Waite JH. Mussel Coating Protein-Derived Complex Coacervates Mitigate Frictional Surface Damage. *ACS Biomater Sci Eng*. 2015;1(11):1121-1128. doi:10.1021/acsbiomaterials.5b00252.

48. Kim S, Yoo HY, Huang J, et al. Salt Triggers the Simple Coacervation of an Underwater Adhesive When Cations Meet Aromatic π Electrons in Seawater. *ACS Nano*. 2017;11(7):6764-6772. doi:10.1021/acsnano.7b01370.

49. Elbaum-Garfinkle S, Kim Y, Szczepaniak K, et al. The disordered P granule protein LAF-1 drives phase separation into droplets with tunable viscosity and dynamics. *Proc Natl Acad Sci USA*. 2015;112(23):7189-7194. doi:10.1073/pnas.1504822112.

50. Danielsen SPO, McCarty J, Shea J-E, Delaney KT, Fredrickson GH. Small ion effects on self-coacervation phenomena in block polyampholytes. *The Journal of Chemical Physics*. July 2019:1-19. doi:10.1063/1.5109045.

51. Waite JH. Mussel adhesion - essential footwork. *J Exp Biol*. 2017;220(Pt 4):517-530. doi:10.1242/jeb.134056.

52. Zhao H, Robertson NB, Jewhurst SA, Waite JH. Probing the adhesive footprints of Mytilus californianus byssus. *Journal of Biological Chemistry*. 2006;281(16):11090-11096. doi:10.1074/jbc.M510792200.

53. Lu Q, Danner E, Waite JH, Israelachvili JN, Zeng H, Hwang DS. Adhesion of mussel foot proteins to different substrate surfaces. *J R Soc Interface*. 2013;10(79):20120759–11. doi:10.1098/rsif.2012.0759.

54. Danner EW, Kan Y, Hammer MU, Israelachvili JN, Waite JH. Adhesion of Mussel Foot Protein Mefp-5 to Mica: An Underwater Superglue. *Biochemistry*. 2012;51(33):6511-6518. doi:10.1021/bi3002538.

55. Yu J, Wei W, Danner E, Israelachvili JN, Waite JH. Effects of Interfacial Redox in Mussel Adhesive Protein Films on Mica. *Adv Mater*. 2011;23(20):2362-2366. doi:10.1002/adma.201003580.

56. Yu J, Kan Y, Rapp M, the EDPO, 2013. Adaptive hydrophobic and hydrophilic interactions of mussel foot proteins with organic thin films. *National Acad Sciences*. doi:10.1073/pnas.1315015110/-/DCSupplemental.

57. Maier GP, Rapp MV, Waite JH, Israelachvili JN, 2015. Adaptive synergy between catechol and lysine promotes wet adhesion by surface salt displacement. *sciencesciencemagorg*. doi:10.1126/science.aab3175.

58. Pashley RM. Hydration forces between mica surfaces in electrolyte solutions. *Advances in Colloid and Interface Science*. 1982;16(1):57-62. doi:10.1016/0001-8686(82)85006-9.

59. Martinez Rodriguez NR, Das S, Kaufman Y, Israelachvili JN, Waite JH. Interfacial pH during mussel adhesive plaque formation. *Biofouling*. 2015;31(2):221-227. doi:10.1080/08927014.2015.1026337.

60. Wei W, Tan Y, Rodriguez NRM, Yu J, Israelachvili JN, Waite JH. A mussel-derived one component adhesive coacervate. *Acta Biomaterialia*. 2014;10(4):1663-1670. doi:10.1016/j.actbio.2013.09.007.

61. Wei W, Petrone L, Tan Y, et al. An Underwater Surface-Drying Peptide Inspired by a Mussel Adhesive Protein. *Advanced Functional Materials*. March 2016:n/a–n/a. doi:10.1002/adfm.201600210.

62. Nicklisch SCT, Waite JH. Mini-review: The role of redox in Dopa-mediated marine adhesion. *Biofouling*. 2012;28(8):865-877. doi:10.1080/08927014.2012.719023.

63. Yu J, Wei W, Danner E, Ashley RK, Israelachvili JN, Waite JH. Mussel protein adhesion depends on interprotein thiol-mediated redox modulation. *Nat Chem Biol*. 2011;7(9):588-590. doi:10.1038/nchembio.630.

64. Nicklisch SCT, Spahn JE, Zhou H, Gruian CM, Waite JH. Redox Capacity of an Extracellular Matrix Protein Associated with Adhesion in Mytilus californianus. *Biochemistry*. 2016;55(13):2022-2030. doi:10.1021/acs.biochem.6b00044.

65. Anderson TH, Yu J, Estrada A, Hammer MU, Waite JH, Israelachvili JN. The Contribution of DOPA to Substrate-Peptide Adhesion and Internal Cohesion of Mussel-Inspired Synthetic Peptide Films. *Advanced Functional Materials*. 2010;20(23):4196-4205. doi:10.1002/adfm.201000932.

66. Cooper LHN. OXIDA TION-REDUCTION POTENTIAL IN SEA WATER By L. H. N. Cooper, Ph.D., F.I.C. *https://doiorg/101017/S0025315400011929*. December 2008:1-10. doi:10.1017/S0025315400011929.

67. Miller DR, Spahn JE, Waite JH. The staying power of adhesion-associated antioxidant activity in Mytilus californianus. *J R Soc Interface*. 2015;12(111):20150614-20150617. doi:10.1098/rsif.2015.0614.

68. Zhao H, Waite JH. Linking adhesive and structural proteins in the attachment plaque of Mytilus californianus. *Journal of Biological Chemistry*. 2006;281(36):26150-26158. doi:10.1074/jbc.M604357200.

69. Inaba K. Structural basis of protein disulfide bond generation in the cell. *Genes Cells*. 2010;15(9):935-943. doi:10.1111/j.1365-2443.2010.01434.x.

70. Yu J, Wei W, Danner E, Ashley RK, Israelachvili JN, Waite JH. Mussel protein adhesion depends on interprotein thiol-mediated redox modulation. *Nat Chem Biol*. 2011;7(9):586-588. doi:10.1038/nchembio.630.

# Chapter II.

## Thiol Rich Layer in the Core-Shell Architectures of byssus threads

Reproduced in part with permission from: Valois, E. and Waite, J.H. (2019). The Thiol-Rich Interlayer in the Shell/Core Architecture of Mussel Byssal Threads. *Langmuir*. **Article ASAP.** DOI: 10.1021/acs.langmuir.9b01844

### A. Abstract

The mussel byssus thread is an extremely tough core-shelled fiber that dissipates substantial amounts of energy during tensile loading. The mechanical performance of the shell is critically reliant on 3, 4-dihydroxyphenylalanine's (Dopa) ability to form reversible iron-catecholate complexes at pH 8. However, the formation of these coordinate crosslinks is undercut by Dopa's oxidation to Dopa-quinone, a spontaneous process at seawater conditions. The large mechanical mismatch between the cuticle and the core lends itself to further complications. Despite these challenges, the mussel byssus thread performs its tethering function over long periods of time. Here we address these two major questions. 1) How does the mussel slow/prevent oxidation in the cuticle and 2) how is the mechanical mismatch at the core-shell interface mitigated? By combining a number of microscopy and spectroscopy techniques we have discerned a previously undescribed layer. Our results indicate this interlayer is thiol rich and thus will be called the thiol-rich interlayer (TRL). We propose the TRL serves as a long-lasting redox reservoir as well as a mechanical barrier.

**B. Introduction.**

Materials with core-shell architectures are pervasive throughout nature and technology. Indeed, in nature there may be no functional material without both core and shell. The utility of a core/shell design is self-evident: the core provides bulk properties e.g. tensile or compressive strength in load bearing materials, while the shell protects the core from corrosion, light, desiccation, microbial attack, and/or abrasion in the ambient environment. Because the disparate functions of shell and core usually lead to incompatibilities between the two, additional adaptive layers are introduced to enhance their union. These are increasingly referred to as self-stratifying coatings [1], and, once again, were evolved by biology, e.g. plant cutins, long before becoming a design concept in engineered materials. Some, but by no means all, biological coatings may thus provide valuable insights for stimulating improvements in manufactured coatings.

Mussel byssal threads have core-shell architectures in which the shell is 5-6 times stiffer than the core[2]. The thread core consists of anisotropic bundles of collagen fibers not unlike tendon, whereas the shell, known as the cuticle, is a composite of granules dispersed in a continuous, amorphous matrix. The granules are largely composed of a Dopa-rich mussel foot protein, which, at pH 5-8, readily binds iron to form cross-linking bis- and tris-catecholate-iron complexes [3,4]. Given the reversible nature of metal-coordinate bonds, tris catecholate-iron complexes are reversible sacrificial bonds, dissipating energy by enabling greater strain during deformation. During unloading, the tris-catecholate-iron complexes self-heal to repair damage sustained during deformation, but only in a Dopa-rich environment[6]. The high dissolved oxygen content and abundance of trace metals make seawater a powerful oxidant of Dopa [7] thus undermining its integrity in byssal threads, yet

Dopa-iron complexes remain stable in the cuticle. How does the mussel protect the cuticle against oxidative damage and consequent loss of function?

Our structural, chemical and nanomechanical analyses of byssal threads suggest that thread redox is maintained by cuticle stratification in combination with thiol enrichment in a subsurface layer, i.e. the thiol rich layer (TRL). A combination of microscopy techniques including transmission electron microscopy (TEM), scanning electron microscopy (SEM) and atomic force microscopy were used to characterize the location and morphology of this TRL. Furthermore, fluorescence microscopy, X-ray near edge spectroscopy (XANES) and secondary ion mass spectrometry were used to speciate the thiol.

Prior studies have identified the cuticle as being significantly stiffer than the core[5]. While this unique combination of stiff cuticle and compliant core results in high toughness, it creates the possibility of contact damage at the interface between the two mechanically mismatched materials. Here, we characterize the nano-mechanical characteristics under biologically relevant conditions using indentation type atomic force microscopy. Although our measurements confirm a large discrepancy in elastic modulus between cuticle and core, they also reveal that the inclusion of the TRL creates a step gradient in hardness and abrasion resistance. By building on many years of byssus research, the present study addresses two major gaps in our understanding. First, how the cuticle copes with an oxidizing environment, and second, how the byssus successfully joins two mechanically mismatched materials.

## C. Materials and Methods

### *TEM/STEM*

Threads less than 48 hours old were excised from the animal and fixed according to the following procedure: All fixation and washing steps were performed on ice. Threads were fixed with 2% formaldehyde, 2.5% glutaraldehyde in fixation buffer (200 mM sodium cacodylate, 300 mM NaCl, pH 7.2) for 2 h. The samples were washed three times (10 min each) in degassed fixation buffer and then post-fixed in 2% osmium tetroxide in degassed fixation buffer for 2 h. The samples were then washed 4 times (10 min each) in degassed deionized water and then dehydrated through a graded series of ethanol washes (25, 50, 75, 90, 100, 100, 100% ethanol, 10 min each). Solvent was then switched to propylene oxide by washing in 33, 66, 100, 100, 100% propylene oxide in ethanol. The samples were then infiltrated with epoxy resin (Embed812, Electron Microscopy Sciences, Hatfield, USA) incubating the sample in resin diluted in propylene oxide as follows: 33% (2 h), 66% (16 h), and 100% (4 h). Finally, samples were placed in molds and cured at 60 °C for 24 h. Thin sections (60–80 nm) for TEM were cut on an EM UC6 ultramicrotome (Leica Biosystems). Sections were mounted on copper TEM grids and post-stained on drops of uranyl acetate and lead citrate following standard protocols. All samples were investigated with a Tecnai G2 transmission electron microscope (FEI) operating at 200 kV, and micrographs were recorded with a Gatan Ultrascan CCD camera (2048 × 2048 pixels. STEM images were acquired using a Titan transmission electron microscope operating at 300 kV. Collagen spacing was calculated using Fiji's (v. 2.0.0-rc-65) nearest neighbor distance (NND) plugin. Prior to analysis, each image was smoothed, and a threshold was applied resulting in a binary image.

### *Atomic Force Microscopy (AFM)*

Images and force measurements were conducted on a MFP-3D Bio (Asylum Research, Santa Barbara, CA). FORTA silicon tips (APPNano, Mountain View, CA) were used in all experiments. Fresh threads (<48 hours old) were imbedded in Neg-50 cryoprotectant (Rachard-Allan Scientific, San Diego, CA) and frozen to -20º C. 10 µm thick sagittal sections were cut using a Leica Cryostat. Sections were placed on top of a drop of water on a poly-lysine slide. The water was subsequently removed with a gel loading pipette tip causing the section to lie flat on the slide. Once mounted, sections were allowed to dry for 1 hour prior to measurement, ensuring sufficient adherence to the slide. 20 $\mu m^2$ topology images were generate using AC mode at a rate of 0.7 HZ. For submerged samples, threads were allowed to equilibrate in seawater for 1 hour prior to imaging. Prior to force measurements, the cantilever spring constant was experimentally determined by the thermal tune method usually ranging between 2 and 3 N/m. Deflection sensitivity was calculated using a glass slide as an indefinitely stiff calibrant material. Force spectroscopic maps of 32X32 pixels were recorded over previously acquired topology images. Force spectroscopy measurements were conducted at 250 nm/s load/unload rate with a maximal loading force of 500 nN. Stiffness and hardness values were calculated by Asylum Research's Elastic Analysis Tool by fitting the upper 1/3 of the loading curve, an indenter half angle of 20 º, and a Poisson ratio of 0.33 to the Hertz Model.

### *SEM*

Fresh threads were fixed with 2% formaldehyde, 2.5% glutaraldehyde in fixation buffer (200 mM sodium cacodylate, 300 mM NaCl, pH 7.2) for 2 h. Fixed threads were

imbedded in Neg-50 cryoprotectant (Rachard-Allan Scientific, San Diego, CA) and frozen to -20º C. 10 μm thick sagittal sections were cut using a Leica Cryostat. Sections were washed 3 times, 10 min each, in milli-Q water to remove any excess cryoprotectant. Solvent exchange from water to ethanol was performed in steps of 30%, 50%, 60%, 90%, 100% X3 ethanol. Samples were dried and secured to aluminum imaging stub with double sided carbon tape. A thin layer of gold-palladium (60:40) was sputter coated onto the sample for 100 seconds using an Anatech USA Hummer 6.2 coater. Specimens were viewed at 3kV with a FEI Nova Nano 650 FEG SEM.

***Fluorescence Microscopy***

Transverse cross sections of fresh mussel threads were prepared as described above. Sections were washed 3 times (1 min each) to remove excess cryoprotectant followed by 3 times 5 min each in phosphate buffered saline (PBS) pH 7.4 (Gibco Life Technologies). Washed sections were incubated in 1μM Alexa $Fluor_{555}$ $C_2$ Maleimide (Thermo Fisher Scientific, Waltham, MA) in PBS for hours at room temperature. Alexa Fluor 555 $C_2$ Maleimide stock was prepared by dissolving received product in dimethyl sulfoxide to a final concentration 10mM. Following staining, sections were rinsed 3 times (10 min each) in PBS to remove excess dye and subsequently mounted onto glass slides using ProLong Gold Antifade Mountant (Thermo Fisher Scientific, Waltham, MA). Confocal images were collected using a Leica SP8 confocal microscope (Leica Microsystems) fitted with 63X/1.4NA oil immersion objective and hybrid detectors (HyD). Thread cuticle was visualized via its intrinsic fluorescence when excited with a 405 nm laser. Alexa $Fluor_{555}$ stained TRL was visualized using the white light laser tuned to 550 nm excitation.

Comparative fluorescent intensity was calculated with Fiji's analyze plot profile function. Alkylation of cysteine residues was accomplished using iodoacetamide (IAM). In control threads, alkylation was done prior to Alexa Fluor$_{555}$ $C_2$ Maleimide addition by incubating thread sections in 60 μM IAM in PBS pH 7.4 for 1 hour.

***Accessory and Collagen Granule Isolation and Tandem MS***

Live *Mytilus californianus* were collected from Goleta Pier in Goleta, CA and stored in maricultural tanks with an open seawater circulation system. Feet were excised from the mussel and sliced into sections approximately 3 mm in length using a No. 10 scalpel. The distal portion of the foot surrounding the distal depression was discarded in order to avoid contamination from phenol gland granules. Gland tissue at the center of the foot was carefully separated from the pigmented epithelium and homogenized in 1mL per foot of 0.05M sodium phosphate pH 7.4 with 0.45M NaCl (mPBS). Granules were separated from insoluble tissue by successive centrifugation through a 40 μm mesh followed by 5 μm mesh (2X 10 min each at 500g). If necessary, additional mPBS was used to rinse the mesh in between spin cycles to prevent clogging. After the final centrifugation, granules were pelleted at 1000g for 10 min and the supernatant was removed. Pelleted granules were resuspended in 0.1M Citrate pH 5.0 with 0.6M Sucrose 0.005M Ascorbic Acid and 0.001M EDTA. Resuspended granules were then subjected to differential centrifugation gradient of 10 to 50% OptiPrep (Alere Technologies, Waltham, MA) for 16 hours at 31,000rpm, 4°C (Beckman L8-80M Ultracentrifuge, Beckman Coulter, Brea, CA). Granules contained in 40% Optiprep were collected for trypsinization. Optiprep was removed from the sample by diluting 1:10 with mPBS and re-pelleted at 1000g for 5 min X 3. Trpysinization was done in

50 mM Tris- HCl (pH 8), 5 mM DTT, and 8 M urea at 37°C for 4 hours. Resulting peptides were sent to UC Davis mass spectrometry facility for sequencing (Davis, CA). Peptides were quantified and 1.0µg was injected into the Xevo G2 QT mass spectrometer coupled to a nano-UPLC system (Waters, Milford, MA. USA). Peptides were injected into a nanoTile, housing a C18 column and eluted off the column in 1h gradient from 2 to 60% acetonitrile. Mass spectrometry analysis was done using MSe, a data independent acquisition (DIA) method. Data analysis was done using Protein Lynx Global Server and subsequently analyzed in Scaffold-4 (Proteome Software, Portland, OR USA)

***µXANES***

For determining in situ sulfur species, synchrotron-based sulfur X-ray absorption near-edge spectroscopy (S XANES) were measured at beamline (BL) 14-3 at the Stanford Synchrotron Radiation Lightsource (SSRL) using a Si(111) (Φ = 90) double crystal monochromator. The monochromator was calibrated at the thiol pre-edge energy of a sodium thiosulfate powder to 2472.02 eV. The fluorescence lines of interest were measured with a Si Vortex Si drift detector (SII Nano Technology) using Xspress3 pulse processing electronics (Quantum Detectors) that deliver superior count rates without significant dead times. The X-ray beam was focused using Kirkpatrick-Baez (K−B) mirrors to a size of ~3 × 3 µm at a flux of ~2 × 1010 photons per second. To determine sulfur speciation at specific points within the sample, absorption spectra (S XANES) were collected from 2460 to 2536 at 0.2 eV steps to capture the range of energies for the absorption edges of possible common sulfur compounds. Multiple spectra were acquired at each point to confirm that the

absorption edge energies did not shift to lower energies because of photoreduction by beam damage to the sample.

### *SIMS*

Sagittal sections of threads less than 48 hours old were excised from the animal and prepared according to TEM procedures. Thin sections were then mounted to a silicon wafer. To ensure a flat sample surface, sections were floated on a small drop of water placed on top of a silicon wafer. The water droplet was slowly evaporated by heating the wafer to 50ºC with a heating block. Elemental mapping was conducted using a Cameca IMS 7f-Auto SIMS. Negative ions ($^{32}S^-$ and $^{26}CN^-$) were mapped with a primary cesium gun using 15 kV impact energy and spot size of 1.5um.

### *DPPH Assay*

Given the light sensitivity of DPPH, all reaction vessels containing DPPH were wrapped in foil. 2mM stock solution was made by resuspending DPPH in 99.5% ethanol. 100µL of stock was added to 900µL of ethanol. The resulting 0.2mM DPPH solution was mixed 1:1 with 0.1M Tris buffer (pH 7.4). 5mg of sectioned threads were added to the solution and mixed by tube inversion. The absorbance at 517 nm was monitored over time. A blank solution was prepared by replacing 100µL stock with 100µL ethanol. As a control, 100µL stock was replaced with 100µM cysteine. The percentage of DPPH remaining was calculated by the following: % remaining = ($Abs_{sample,t}/Abs_{control,t}$ x 100)

## D. Results

### *Ultrastructural characterization of distal byssus*

Transverse cross-sections of distal byssal threads from local *Mytilus californianus* reveal the three distinct regions: 1) cuticle, 2) TRL and 3) core. The granular structure of the cuticle is readily visible with TEM and is characterized by the presence of ~500 nm (diam) electro-lucent granules surrounded by an electron-dense protein matrix at a fill ratio of 1:1 (Figure 2.1.B) [8]. Granules are the primary location of iron-catecholate complexes in the byssal thread [4] and function to increase the abrasion resistance of the exterior coating and prevent dehydration during times of exposure to atmosphere [8]. The core of each byssal thread consists of anisotropic microbundles of collagen fiber bundles oriented parallel to the long axis of the thread (Figure 2.1.C,D,E). In this study, high resolution transmission electron microscopy (STEM) was employed to measure an average diameter of 13.6 ± 1 nm (Figure 2.2).

Sandwiched between the cuticle and core, an electron dense homogenous material is discernable. We shall refer to this as the thiol rich layer (TRL). However, as revealed by STEM, true homogeneity is complicated by interfacial penetration of TRL by collagen fibers Figure 1C). Fibers within the TRL maintain a diameter similar to that of the core, 13.6 ± 0.7 nm (Figure 2.2.B,C). Furthermore, fibrillar center to center distance, indicative of collagen packing density, remains unchanged; 22.3 and 23.7 nm for the TRL and core, respectively. We interpret this to mean that collagen in the TRL is not significantly different from that of the core.

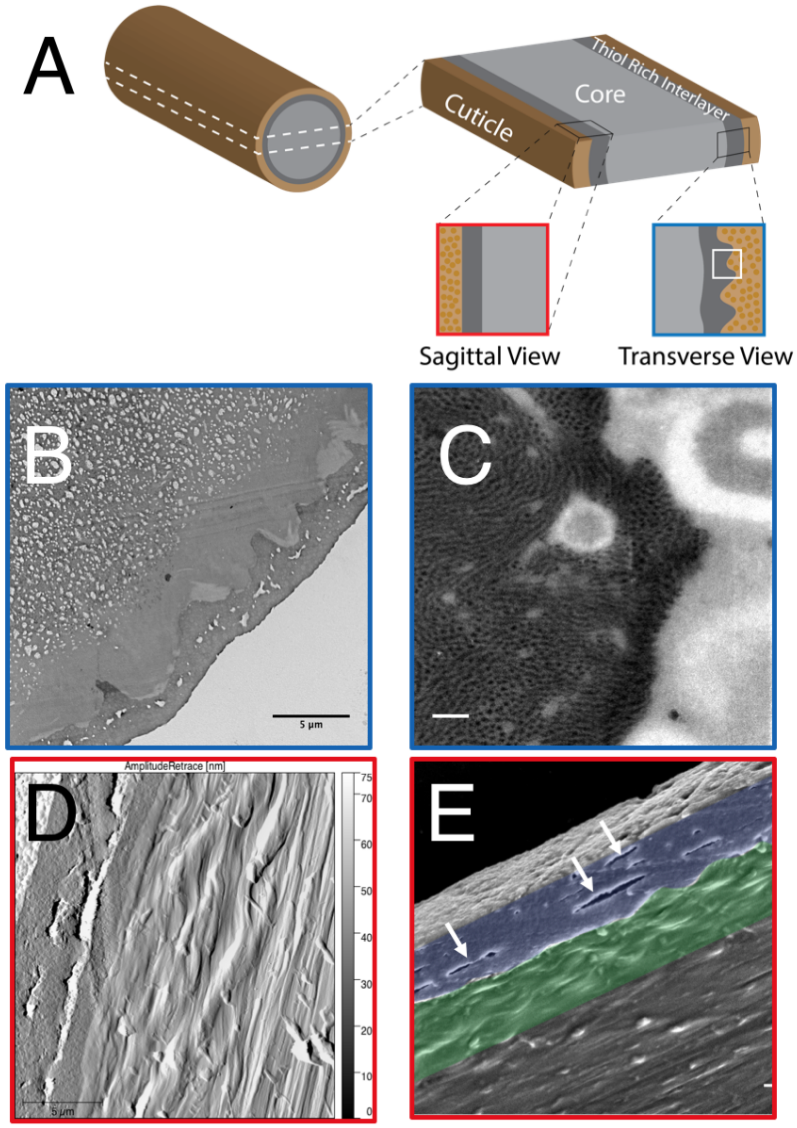


*Figure 2.1. Byssal thread cross sections. B & C are transverse cross sections. D and E are sagittal cross sections. A) Illustration of mussel byssal thread components and location. B) Transmission electron micrograph of transverse section of mussel byssus thread in which the cuticle, TRL and core are visible moving from bottom to top. Scale bar is 5 µm. C) Zoom of TRL as observed in STEM. Representative region of C is shown by white box in A. Scale bar is 100nm. D) AFM amplitude image of a sagittal section of the byssal thread. Moving from left to right, the cuticle, TRL and core are all visible. Scale bar is 5 µm. E) SEM of the byssal thread section. Visible are circumferential cracks/voids in the cuticle (white arrows), the 'wavy' interphase (green) and fibrous core (black). Scale bar is 5 µm.*

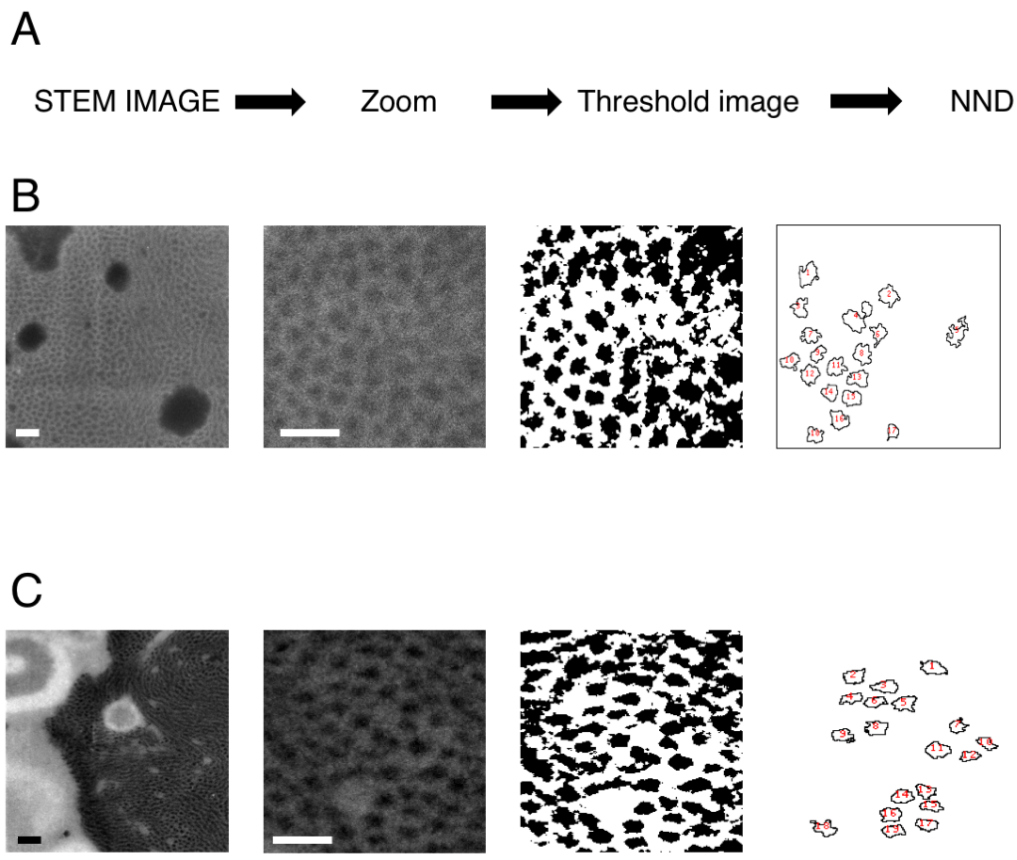


*Figure 2.2. STEM images used for collagen bundle size and spacing calculation. A) Workflow diagram used to process acquired STEM images. B) Core images. C) Interphase Images. Scale bars for left most panels are 100 nm. Scale bars for second panel from the left is 50 nm.*

In thin (<100nm) transverse sections, collagen bundles contained in the TRL appear to maintain their anisotropy. However, imaging of sagittal cross sections demonstrates that fibers in the TRL are more isotropic (Figure 2.1D). Furthermore, voids and cracks that form in

the cuticle as the result of normal deformation become visible. Interestingly, these cracks are deflected by the TRL and only propagate parallel to the long axis of the fibers (Figure 2.1.E).

***Biochemical Characterization:***

The byssal thread is formed by a processive injection molding of secretory vesicles from two specific glands in the ventral groove of the foot [11]. The collagen gland contains prolate ellipsoid vesicles containing collagen mesophases, which self-assemble into mature collagen fibers during molding of the core (Figure 2.3.A-E). The coating or cuticle is formed when the accessory gland secretes spherical vesicles with a "marbled" internal structure [11] that flow over and coat the nascent collagen core. Recently, in-depth analysis of the accessory gland transcriptome revealed, at the mRNA level, the presence of four novel mussel foot proteins (mfp's); mfp -16, -17, -18, -19. This cohort of mfps contained cysteine levels ranging from 7 to 20 mole percent[12]. By isolating cuticle and collagen vesicles from their respective glands, we directly confirmed one of the aforementioned proteins (Figure 2.3.F). A dispersion of granules prepared from the accessory gland was trypsinized and subjected to ESI-TOF-MSMS. A positive identification of the sequence HDDYSSDPYTEPQK was made to residues 85-99 of a 21-kDa protein, mfp-17[12]. Full cysteine-enriched sequence is shown in Figure 2.3.H. Sequences for other proteins known to exist in the isolated secretory

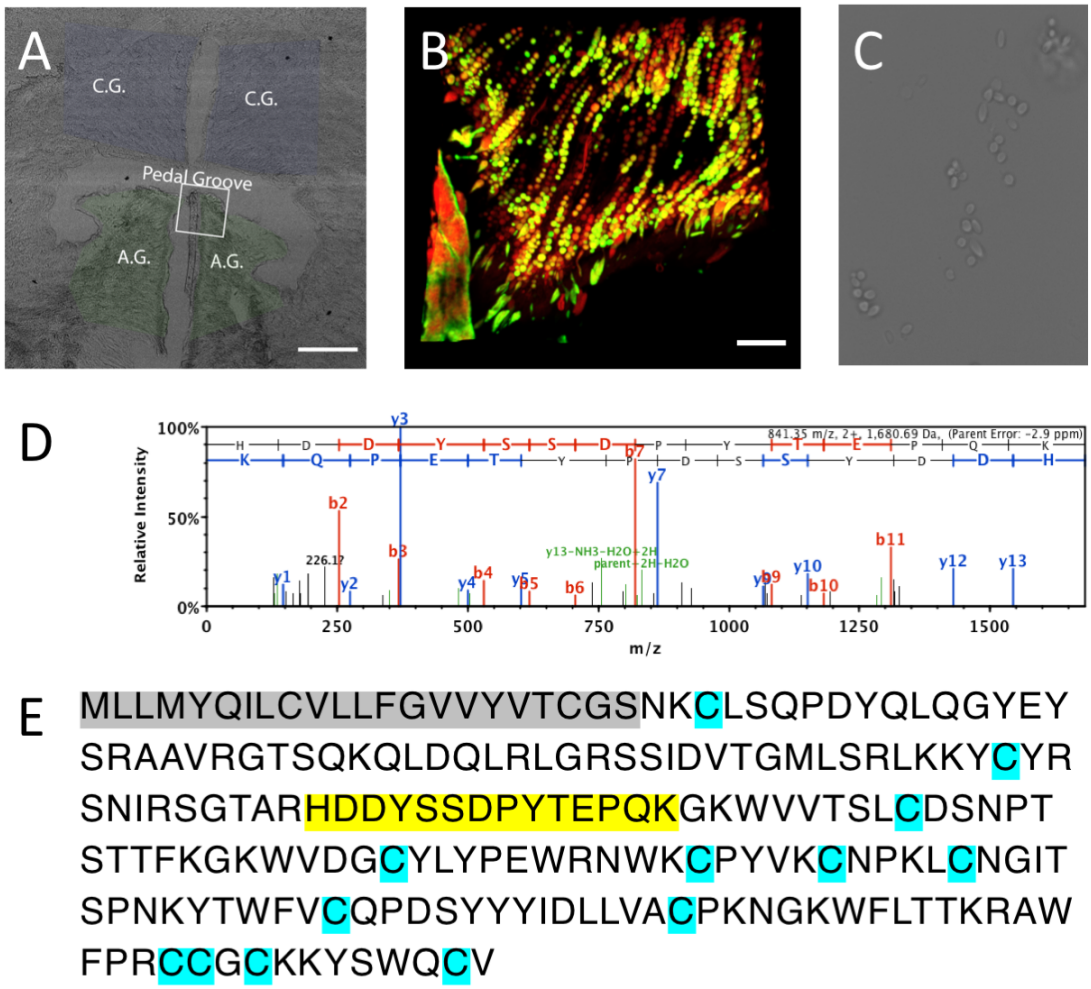


*Figure 2.3.*

*Localization of secretory granules in the foot of M. californianus. A) Optical micrograph of overview of the foot cross section. Gland tissues have been labeled according to the contained granule type. C.G. is the collagen gland which contains granules of pre-Col. A.G. is the accessory gland which stores cuticle precursors. White box region is shown expanded in panel B. Scale bar is 100 µm; B) Overlay of fluorescence micrograph using 405 nm excitation (Red, intrinsic protein fluorescence) and 550nm excitation (Green, thiol specific Alexafluor 555 $C_2$ Maleimide). Scale bar is 10 µm. C) Optical micrograph of granules isolated from the foot by differential centrifugation. Circular granules contain cuticle precursors and are stored in the accessory gland. Prolate vesicles contain pre-Col. D) MSMS spectra used for identification of mfp-17 (yellow) in complete sequence of mfp-17 (E)*

vesicles, namely preCol-D and preCol-NG are shown in supplemental figures 6 and 7, respectively.

Thin (10μm) transverse sections were incubated with Alexafluor 555 $C_2$ Maleimide, a cysteine specific fluorescent reporter and subjected to confocal fluorescent microscopy. When illuminated with 550nm light, the ~5μm region identified as the TRL fluoresces (Figure 2.4B,C) and agrees with earlier detection of sulfur enrichment by electron dispersive X-ray spectroscopy[13]. Whereas the core exhibits small degrees of fluorescence, attributed to a single cysteine residue in each preCol-D chain, the intensity in the TRL is 250% higher (Figure 2.4D). Thiol-maleimide Michael addition is necessarily dependent upon thiolate formation under pH conditions at or above the thiol $pK_a$ – typically >7. Accordingly, the evolution of fluorescence in the TRL suggests that prior to maleimide addition, cysteine side chains are not engaged as disulfides. To confirm the presence of cysteine, not cystine, micro-X-ray absorption near edge spectroscopy (μXANES) at the sulfur K-edge was conducted. Sulfur XANES is a powerful tool for chemical characterization in complex biological systems and is particularly well suited for determination of sulfur speciation due to large chemical shift ranges and sharp line widths [14]. The TRL has an absorption maximum centered at 2473.59 eV, characteristic of sulfur with a -2 oxidation number [15] and consistent only with reduced thiols (Figure 2.4E).

Surprisingly, the cuticle exhibited no signs of cysteine in either fluorescence microscopy (FM) or XANES. Because the oxidation state of sulfur has a profound effect on detection by both techniques, it was important to verify the results with a third technique that is independent of oxidation state. Secondary Ion Mass Spectrometry (SIMS) provides element specific mapping at 1μm resolution with sensitivity in the singles of ppb, but most

importantly, is unaffected by oxidation state[16]. By bombarding a thread section with $^{133}Cs^{+}$, the generation of $^{32}S^{-}$was monitored and mapped to the sample surface. Concurring with FM and XANES, sulfur levels in the cuticle were below the detectable limit (Figure 2.5) .

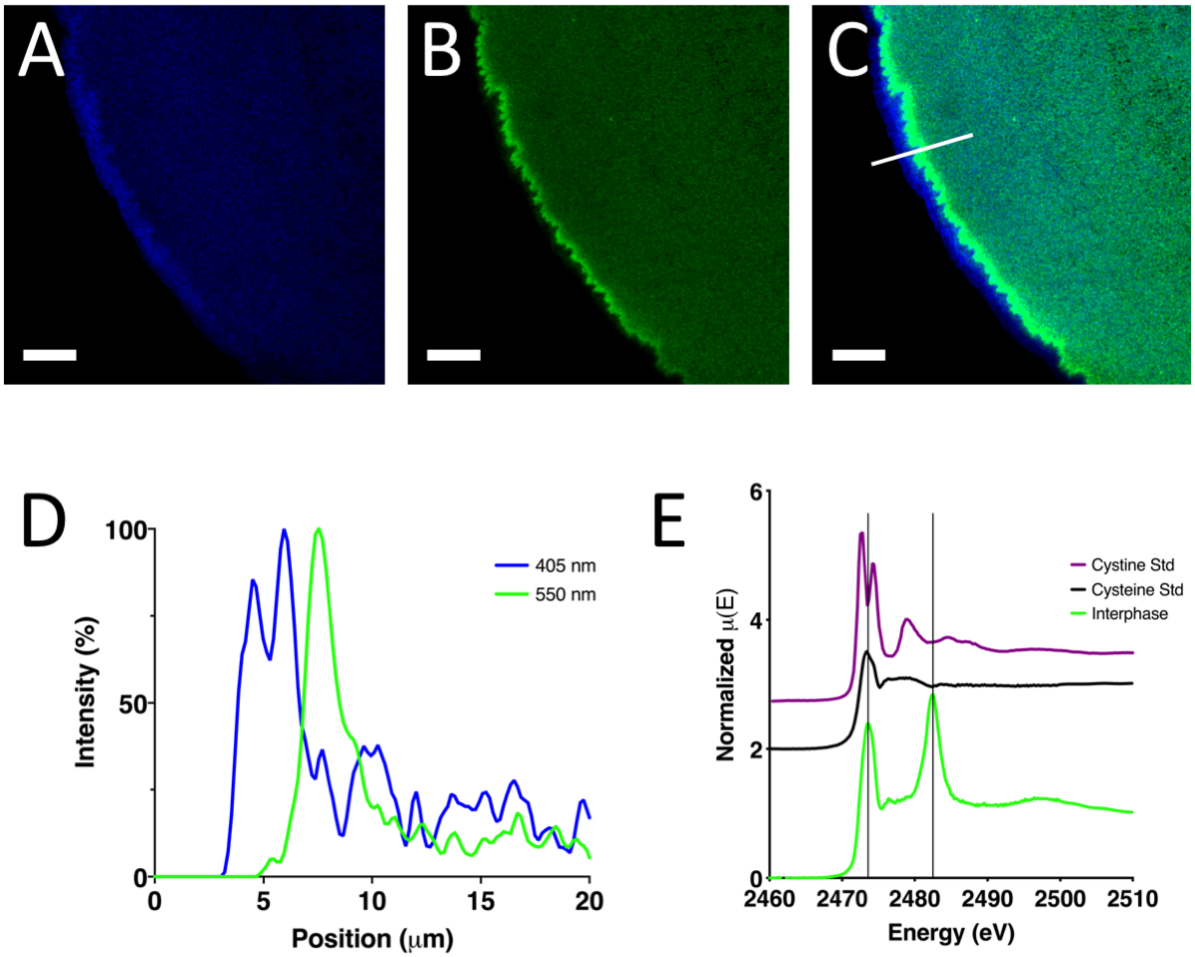


*Figure 2.4 Localization of cysteine residues in the thread. A-C) Fluorescent micrographs of transverse cross sections at varying excitation wavelengths. A) excitation at 405 nm used to visualize the cuticle. B) Excitation at 550 nm. C) Overlay of A and B. Scale bars in A-C are 10 μm D) Intensity profile of fluorescence from white line in C. E) XANES spectra of the interphase (green) vs cysteine (black) and cystine (purple) standards.*

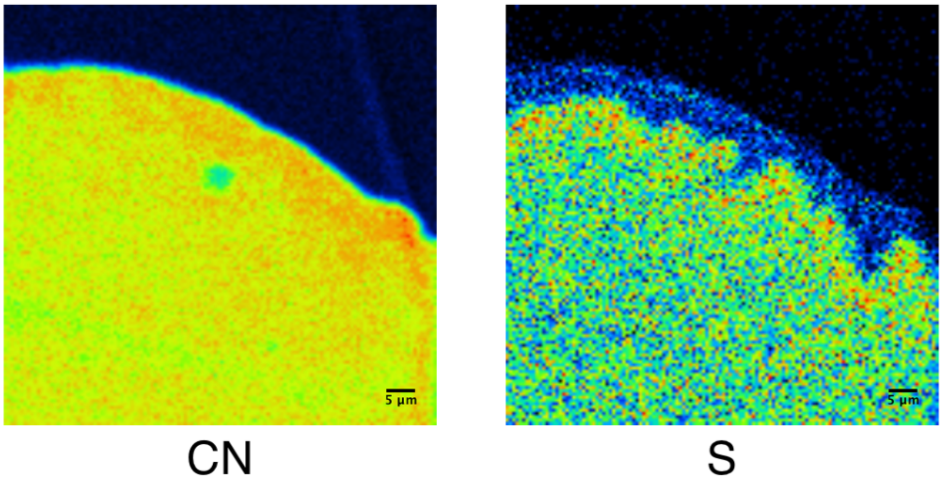


*Figure 2.5 Secondary Ion Mass Spectrometry images. Left) Carbon-Nitrogen ($^{26}CN^-$) was used as a fiducial marker for protein backbones allowing for the entire thread cross section to be visualized. Right) $^{32}S^-$ map demonstrating depauperate sulfur in the cuticle whereas sulfur is concentrated in the TRL and moderate in the core.*

***Reducing Capability*:**

The average standard redox potential of $O_2$ in seawater is ~600mV SHE, substantially higher than that of DOPA contained in mfps [17], making the coupling of oxygen reduction with DOPA oxidation a likely event. DOPA oxidation to DOPAquinone compromises its ability to form the metal coordinate complexes, which are essential to the cuticle's cohesion and self-healing behavior [2,18,19]. The high cysteine density of the TRL provides the cuticle with a dedicated redox reservoir which can be called upon in times of increased oxidative stress. The antioxidant capacity of the byssal thread was probed using the redox dye 2,2-diphenyl-1-picrylhydrazyl (DPPH). DPPH absorbs maximally at 517 nm in its oxidized form[20,21], however, bleaching occurs when exposed to a reducing agent such as cysteine. Incubation of byssal thread cross sections with DPPH reveals a sustained antioxidant

capacity ($t_{1/2}$ ~100min) (Figure 2.5). By comparison, free cysteine lost 50% of its reducing capacity in <5 minutes. To demonstrate that cysteine side chains in thread proteins are the primary source of reducing equivalents, thread cross sections were treated with iodoacetamide (IAM) prior to the DPPH assay. IAM modification of cysteinyl-thiol produces cysteine-S-acetamide, which is incapable of DPPH reduction. The resulting assay yielded a less than 3% decrease in DPPH absorption over 60 min, confirming that thiols are the major primary reductant in the thread.

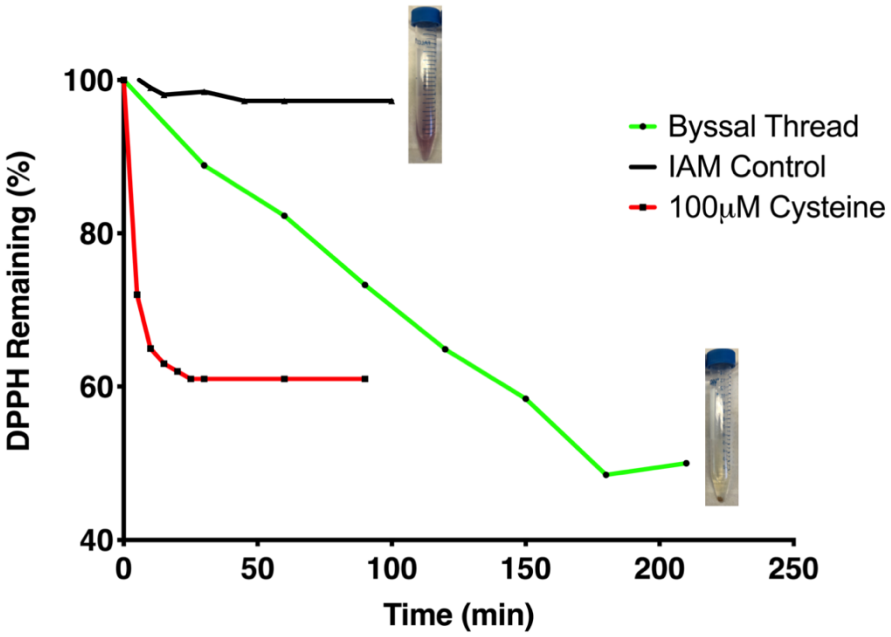


*Figure 2.6. DPPH Assay. Sustained redox activity is observed in byssal threads (Green) whereas the cysteine control quickly reduces the DPPH (Red). When treated with iodoacetamide (IAM) to block cysteine and prevent DPPH reduction, no change is observed in oxidized DPPH levels (Black).*

**Mechanics**:

Position-specific mechanics were probed using indentation type atomic force microscopy (IT-AFM). IT-AFM provides two key advantages compared with other mechanical testing methods. 1) By overlaying topology imaging with force-spectroscopy mapping (FM) one can obtain location specific mechanics with a spatial resolution approaching 10 $nm^2$. 2) The sample testing environment can easily be changed without removing the sample. This is of particular interest to the mussel thread which experiences both wet and dry conditions in nature. This study is the first to probe location specific nano-mechanics while submerged in seawater.

In IT-AFM, the probe is rastered across a previously generated topology image, generating a force vs displacement curve at each pixel. The result is a 2D array of Force vs Displacement curves (FM) from which the modulus and hardness at each pixel are extracted. Under dry conditions, force-spectroscopy maps reveal a shallow gradient of increasing stiffness from the core (1.05 GPa n=1052) to the TRL (1.12 GPa n=1298) to the cuticle (1.28 GPa n=1040) (Figure 2.7A,C).

By switching the testing environment from dry to submerged, dramatically different mechanical behavior emerges. When submerged in seawater, the cuticle stiffness decreases 2.25-fold to ~550 ± 106 MPa. Once hydrated, the TRL and core soften 25-50-fold to 45 ± 7 and 20 ± 5 MPa, respectively (Figure 2.7B,C).

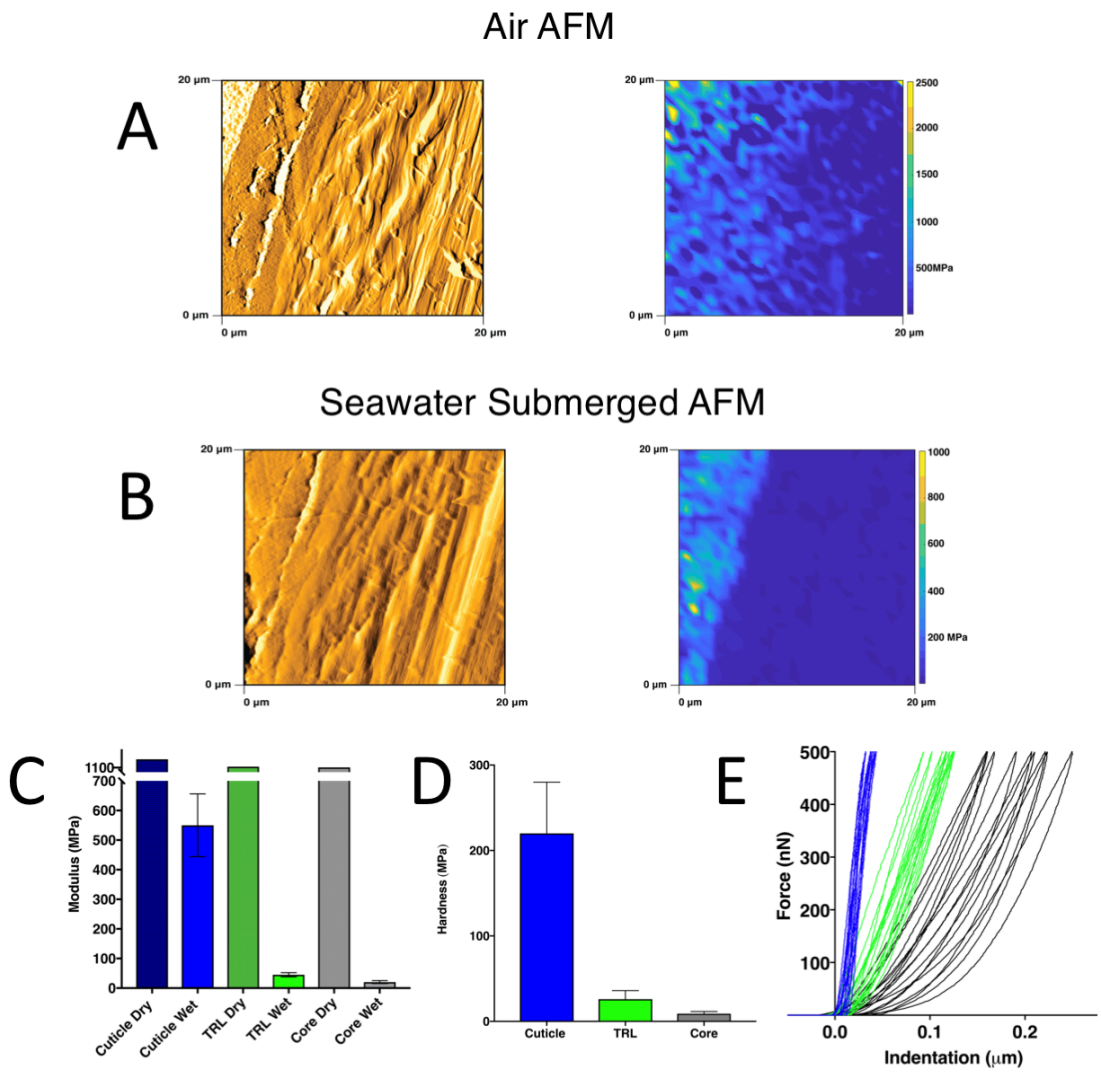


*Figure 2.7. Location specific mechanics as measured by indentation-type atomic force microscopy. A) Amplitude image of a dry sagittal section (left) and associated force spectroscopy map (right). B) amplitude image of sagittal sections submerged in seawater and associated force spectroscopy map (right). For spectroscopy maps, darker blue indicates lower modulus. C) Elastic Modulus of the cuticle, TRL and core under wet and dry conditions. D) Hardness values extracted from Force vs Indentation profiles from submerged samples shown in B. E) 10 Representative F vs I profiles from each hydrated region. Cuticle (blue), TRL (green), core (black).*

Functional gradients are designed to create high-performance materials by confining and insulating specific compositions and architectures to regions of need [22]. As is the case with most core-shelled fibers, the shell is usually designated as a protective outer coating. Consistent with this, the mussel cuticle's stiff granular structure has a hardness (H) of 220 ± 60 MPa (Figure 2.7D). Using Ashby plots of critical properties, the abrasion resistance of a material can be comparatively assessed by plotting H vs E. Materials which fall on a straight line of slope 2/3 have equivalent performance and can be grouped according to their $H^3/E^2$ [23]. The cuticle 'H' and 'E' yield a $H^3/E^2$ of 35 MPa, putting it in the realm of most engineering epoxies. In the TRL, both E and H decrease by an order of magnitude to 26 ±10 MPa. However, the resulting $H^3/E^2$ is 9MPa, only a 4-fold decrease from the cuticle. Given that the core's primary function is to dissipate tensile energy, the need for hardness is not readily apparent. Fittingly, the measured hardness of the core is 9MPa, with a $H^3/E^2$ of 1.5 MPa.

**E. Conclusion:**

Prior studies have classified the byssal thread as a coated, fiber-filled composite material with distinct shell and core domains. By combining microscopy, spectroscopy and mechanical analysis techniques we introduce a third, multi-functional thiol rich layer. The TRL is an approximately 5 $\mu$m thick region intercalated between the cuticle and core and characterized by an increase in cysteine density compared with the two adjoining domains. Additionally, we show that cysteine residues in the TRL persist in their reduced state. Cysteine clustering has been shown in a number of proteins and often increases in proteins designed to deal with high oxidative stress [24], such as that experienced by the byssus. Given

that the mechanical performance of the cuticle necessarily relies on Dopa's ability to form tris-Dopa-iron complexes, which deteriorate upon Dopa oxidization, we propose that the TRL provides a reservoir of electrons to create a sustained reducing environment to protect the cuticle against oxidative damage. Despite being submerged in seawater for 24-48 hours, the threads used for these studies indicated no cysteine oxidation. Further studies to investigate the aging process of the TRL are underway. Given its thiol rich nature, the formation of a variety of covalent bonds including disulfide and cysteinyl-dopa[25] adducts are possible over time. The penetration of collagen fibers into this dense thiol-rich matrix creates a mechanically distinct barrier between the cuticle and the core. The inclusion of this interlayer forms a step gradient in hardness and abrasion resistance from the cuticle to the core which helps mitigate contact damage. Furthermore, composite structures of stiff outer materials underlaid by a gradient of compliant materials favor superficial circumferential cracking as opposed to deep penetrating radial cracking [22]. Prevention of radial cracking prevents cracks from entering the core, which would result in catastrophic failure under tension. The multifunctionality of the TRL addresses two major problem areas of the mussel byssus; oxidation and mechanical mismatch. By further understanding the role of redox chemistry at biological interfaces, we gained valuable knowledge, which may lead to smart design principles for layered load bearing materials.

## F. References


(1) Beaugendre, A.; Degoutin, S.; Bellayer, S.; Pierlot, C.; Duquesne, S.; Casetta, M.; Jimenez, M. Self-Stratifying Coatings: a Review. *Progress in Organic Coatings* **2017**, *110*, 210–241.

(2) Holten-Andersen, N.; Waite, J. H. Mussel-Designed Protective Coatings for Compliant Substrates. *J. Dent. Res.* **2008**, *87* (8), 701–709.

(3) Taylor, S. W.; Chase, D. B.; Emptage, M. H.; Nelson, M. J.; Waite, J. H. Ferric Ion Complexes of a DOPA-Containing Adhesive Protein From Mytilus Edulis. *Inorg. Chem.* **1996**, *35* (26), 7572–7577.

(4) Harrington, M. J.; Masic, A.; Holten-Andersen, N.; Waite, J. H.; Fratzl, P. Iron-Clad Fibers: a Metal-Based Biological Strategy for Hard Flexible Coatings. *Science* **2010**, *328* (5975), 216–220.

(5) Holten-Andersen, N.; Fantner, G. E.; Hohlbauch, S.; Waite, J. H.; Zok, F. W. Protective Coatings on Extensible Biofibres. *Nat Mater* **2007**, *6* (9), 669–672.

(6) Xu, Z. Mechanics of Metal-Catecholate Complexes: the Roles of Coordination State and Metal Types. *Scientific Reports* **2013**, *3* (1), 216–217.

(7) Cooper, L. H. N. OXIDA TION-REDUCTION POTENTIAL in SEA WATER by L. H. N. Cooper, Ph.D., F.I.C. *https://doi.org/10.1017/S0025315400011929* **2008**, 1–10.

(8) Monnier, C. A.; DeMartini, D. G.; Waite, J. H. Intertidal Exposure Favors the Soft-Studded Armor of Adaptive Mussel Coatings. *Nature Communications* **2018**, 1–9.

(9) Hassenkam, T.; Gutsmann, T.; Hansma, P.; Sagert, J.; Waite, J. H. Giant Bent-Core Mesogens in the Thread Forming Process of Marine Mussels. *Biomacromolecules* **2004**, *5* (4), 1351–1355.

(10) Krauss, S.; Metzger, T. H.; Fratzl, P.; Harrington, M. J. Self-Repair of a Biological Fiber Guided by an Ordered Elastic Framework. *Biomacromolecules* **2013**, *14* (5), 1520–1528.

(11) Priemel, T.; Degtyar, E.; Dean, M. N.; Harrington, M. J. Rapid Self-Assembly of Complex Biomolecular Architectures During Mussel Byssus Biofabrication. *Nature Communications* **2017**, *8*, 1–12.

(12) DeMartini, D. G.; Errico, J. M.; Sjoestroem, S.; Fenster, A.; Waite, J. H. A Cohort of New Adhesive Proteins Identified From Transcriptomic Analysis of Mussel Foot Glands. *J. R. Soc. Interface* **2017**, *14* (131), 20170151–14.

(13) Sun, C.; Waite, J. H. Mapping Chemical Gradients Within and Along a Fibrous Structural Tissue, Mussel Byssal Threads. *Journal of Biological Chemistry* **2005**, *280* (47), 39332–39336.

(14) Hullebusch, E. V.; Rossano, S.; Farges, F.; Lenz, M.; Labanowski, J.; Lagarde, P.; Flank, A.-M.; Lens, P. Sulfur K-Edge XANES Spectroscopy as a Tool for Understanding Sulfur Chemical State in Anaerobic Granular Sludge. *J. Phys.: Conf. Ser.* **2009**, *190*, 012184–012185.

(15) Almkvist, G.; Boye, K.; Persson, I. K-Edge XANES Analysis of Sulfur Compounds: an Investigation of the Relative Intensities Using Internal

Calibration. *J. Synchrotron Rad (2010). 17, 683-688 [doi:10.1107/S0909049510022946]* **2010**, 1–6.

(16) Ray, S.; Shard, A. G. Secondary Ion Mass Spectrometry of Proteins. *International Journal of Physical and Mathmatical Sciences* **2011**, *5* (4), 552–556.

(17) Waite, J. H. Mussel Adhesion - Essential Footwork. *J. Exp. Biol.* **2017**, *220* (Pt 4), 517–530.

(18) Li, Y.; Wen, J.; Qin, M.; Cao, Y.; Ma, H.; Wang, W. Single-Molecule Mechanics of Catechol-Iron Coordination Bonds. *ACS Biomater. Sci. Eng.* **2017**, *3* (6), 979–989.

(19) Zeng, H.; Hwang, D. S.; the, J. I. P. O.; 2010. Strong Reversible Fe3+-Mediated Bridging Between Dopa-Containing Protein Films in Water. *National Acad Sciences*.

(20) Nicklisch, S. C. T.; Waite, J. H. Optimized DPPH Assay in a Detergent-Based Buffer System for Measuring Antioxidant Activity of Proteins. *MethodsX* **2014**, *1*, 233–238.

(21) Shimamura, T.; Sumikura, Y.; Yamazaki, T.; Tada, A.; Kashiwagi, T.; Ishikawa, H.; Matsui, T.; Sugimoto, N.; Akiyama, H.; Ukeda, H. Applicability of the DPPH Assay for Evaluating the Antioxidant Capacity of Food Additives - Inter-Laboratory Evaluation Study -. *Anal Sci* **2014**, *30* (7), 717–721.

(22) Liu, Z.; Meyers, M. A.; Zhang, Z.; Ritchie, R. O. Functional Gradients and Heterogeneities in Biological Materials: Design Principles, Functions, and Bioinspired Applications. *Progress in Materials Science* **2017**, *88*, 467–498.

(23) Moses, D. N.; Mattoni, M. A.; Slack, N. L.; Waite, J. H.; Zok, F. W. Role of Melanin in Mechanical Properties of Glycera Jaws. *Acta Biomaterialia* **2006**, *2* (5), 521–530.

(24) Poole, L. B. The Basics of Thiols and Cysteines in Redox Biology and Chemistry. *Free Radical Biology and Medicine* **2015**, *80*, 148–157.

(25) Nicklisch, S. C. T.; Spahn, J. E.; Zhou, H.; Gruian, C. M.; Waite, J. H. Redox Capacity of an Extracellular Matrix Protein Associated with Adhesion in Mytilus Californianus. *Biochemistry* **2016**, *55* (13), 2022–2030.

# Chapter III

## Phase-separated Redox Batteries in Mussel Adhesion

Reproduced in part with permission from: Valois, E. and Waite, J.H. (2019). Phase-separated Redox Batteries in Mussel Adhesion. *Science Advances*. **Article ASAP.** DOI: XXXXXXXXXXXX.

### A. Abstract

Catecholic 3, 4-dihydroxyphenylalanine (Dopa) residues in mussel foot proteins (mfp) contribute critically to mussel (*Mytilus californianus*) plaque adhesion, but only if protected from oxidation at the adhesive-substratum interface. Dopa oxidation is thermodynamically favorable in seawater yet barely detectable in plaques, therefore we investigated how plaques insulate Dopa-containing mfps against oxidation. Seawater sulfate triggers a mfp3 and mfp6 liquid-liquid phase separation (LLPS). By combining plaque cyclic voltammetry with electrophoresis, mass spectrometry and redox exchange chemistry, we show that Dopa-containing mfp3 and mfp6 in phase-separated droplets remain stable despite rapid oxidation in the equilibrium solution. The results suggest that a cohort of oxidation-prone proteins is endowed with phase-dependent redox stability. Moreover, in forming LLPS compartments, Dopa-proteins become reservoirs of chemical energy.

## B. Introduction

Liquid-liquid phase changes in biomacromolecular assemblages are not confined to living cells where they facilitate dynamic compartmentalization associated with time- and location-specific reactions (*1*). A common extracellular and extra-organismic liquid-liquid phase change known as coacervation is involved in the formation of biomolecular materials as diverse as arteries (*2*), silks (*3*), beaks (*4*), butterfly wings (*5*), and marine adhesives (*6,7*). The formation of adhesive plaques by mussels (*Mytilus californianus)* involves a cohort of mostly disordered proteins known as mussel foot proteins (*mfps*) (*8*). Several *mfps* exhibit liquid-liquid phase separation (LLPS) (*7, 9-11*) triggered by specific chemical cues in the ambient seawater. Adaptive advantages of coacervation include concentrating adhesive proteins as fluids, shear thinning to facilitate fluid transport, and low interfacial energy for spontaneous spreading underwater (*4, 9, 12-13*).

An iconic chemical feature of all *mfp*s is 3, 4-dihydroxyphenyl-L-alanine (Dopa), a catecholic amino acid that is post- or co-translationally introduced into the proteins prior to deposition onto target surfaces. Dopa contributes significantly to wet adhesion but only when redox poise is locally controlled. Under reducing conditions (Fig. 3.1), Dopa-containing proteins dehydrate surfaces, form stable π-cation interactions and bidentate H-bonds, coordinate with metal ions and metal oxide surfaces, and, in synergy with lysine, evict adsorbed salts from rock surfaces (*14, 15*). Under oxidizing conditions, Dopa becomes a quinone with strong cross-linking tendencies, but metal oxide/mineral surface binding and metal ion complexation are significantly diminished (*15*) (Fig. 3.1). Known interim adaptations to reduce oxidative losses, including electron-withdrawing effects on the catechol moiety (*16*), surface deposition of mfps at acidic pH (*17-18*) and cosecretion of

mfps with antioxidants (*18-19*), are effective in temporarily optimizing adhesion under experimental conditions, but do not reveal how the long term interfacial redox poise of plaques is maintained in highly oxidizing natural seawater (*20*). In situ probes indicate that the acidic pH of nascent plaques only lasts a few minutes before equilibrating to seawater pH8 (*17*) and yet adhesive interfaces between plaques and substrata remain reducing for months in seawater (*21*).

Using Dopa as an intrinsic redox reporter, we investigated which proteins undergo phase separation in mature plaques and how the phase affects Dopa redox. Given reports of liquid-liquid phase separation in organelle formation and pathogenesis in cells (*1, 22*), the significance of phase-specific redox is likely to extend beyond mussel adhesion.

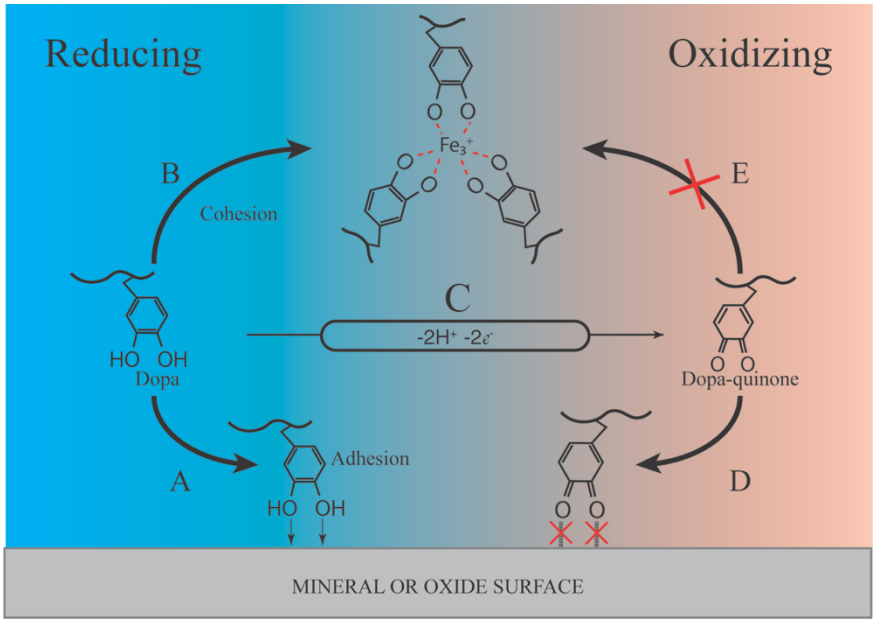


*Figure 3.1. Role of DOPA in mussel foot proteins. A. Dopa-containing mussel foot proteins (squiggle) recruited for adhesion by chemisorption (A) and cohesion by tris-catecholato $Fe^{3+}$ complexation (B). Dopa oxidized by $O_2$ (C) becomes Dopaquinone, which forms covalent adducts but shows reduced surface binding (D) and coordination (E)*

## C. Materials and Methods.

### *Plaque collections*.

California mussels *Mytilus californianus* Conrad harvested from Goleta Pier (34.414088, -119.828690) were held in tanks with circulating natural seawater at 12-16˚C. To prepare the intact mussel plaques for analysis (Figure 1b), the mussels were tethered over target substrates such as mica coated with nanometer thick gold films, mica, glass slides or, for easy sectioning, Saran™ wrap. In the case of gold plated mica, the gold layer remained firmly attached to the plaque but was easily detached from mica surface by gentle tension on the plaque. This approach keeps intact the interfacial plaque chemistry and structure.

### *Transmission electron microscopy of phase transitions.*

All plaques intended for TEM were collected from the same individual and deposited onto Saran™ wrap. Half were processed directly for electron microscopy after optimizing the fixation conditions. Half were placed in 5% acetic acid (15˚C) for 30 min before processing. All fixation and washing steps were performed on ice. Fresh plaques were fixed in 2% formaldehyde, 2.5% glutaraldehyde, and fixation buffer (200mM sodium cacodylate, 300mM NaCl, pH 7.2) for 2 h. The samples were washed three times (10 min each) in degassed fixation buffer and then post-fixed in 2% osmium tetroxide in degassed fixation buffer for 2 h. The samples were then washed 4 times (10 min each) in degassed deionized water and then dehydrated through a graded series of ethanol washes (25, 50, 75, 90, 100, 100, 100% ethanol, 10 min each). Solvent was then switched to propylene oxide by washing in 33, 66, 100, 100, 100% propylene oxide in ethanol. The samples were then infiltrated with epoxy resin (Embed812, Electron Microscopy Sciences, Hatfield, USA) incubating the

sample in resin diluted in propylene oxide as follows: 33% (2 h), 66% (16 h), and 100% (4 h). Finally, samples were placed in molds and cured at 60 °C for 24 h. Thin sections (60–80 nm) for TEM and semithin sections (300 nm) for electron tomography were cut on a EM UC6 ultramicrotome (Leica Biosystems). Sections were mounted on copper TEM grids and post-stained on drops of uranyl acetate and lead citrate following standard protocols (*30*). All samples were investigated with a Tecnai G2 transmission electron microscope (FEI) operating at 200 kV, and micrographs were recorded with a Gatan Ultrascan CCD camera (2048 Å~ 2048 pixels).

***Cyclic Voltammetry***

Cyclic voltammetry was performed at room temperature on a Versastat 3 Potentiostat (Ametek Co) with a typical three-electrode cell using Pt wire as the counter electrode, Ag/AgCl reference electrode, and gold or glassy carbon (3mm disc electrodes from BASi, W Lafayette, IN) as the working electrode at 22˚C and 1 ATM pressure. To avoid interference by adsorbed chemicals on the surface of the working electrode, the following cleaning method was applied to gold electrodes before each experiment: 1) mechanical polishing of the electrode was done using a diamond particle abrasion solution of 1µm, 0.25µm and 0.05 µm particle sizes (Buehler, Lake Bluff, IL) for 2min each on a nylon disk. The electrode was rinsed with water and sonicated for 2min in a shallow vessel containing water to remove excess diamond particles; 2) The electrode was then stripped by repetitive cycling between -400 to +1400 mV (vs. Ag/AgCl) at a rate of 100 mV/s in 50 mM sulfuric acid until the CV became stable (typically 12 cycles). For abrasive polishing of glassy carbon electrodes, diamond particles were replaced with alumina particles of equivalent size.

Analyte autoxidation was minimized by performing all electrochemical experiments with degassed deionized water in a glove-bag under argon. Some CV measurements required notable adaptations: for detached plaques, for example, we used dialysis membranes (Spectrapor MWCO 1000) with 2 O-rings to affix the plaque interface against the working electrode. For reconstituted coacervates, the reference electrode was enclosed in a sleeve of dialysis tubing. Without it, adsorbed coacervates caused significant drift.

**Electro-transfer of Plaque Proteins.** To capture proteins undergoing a phase change from a condensed state to solution, plaques naturally deposited by mussels onto glass slides (Fisher Scientific 12-544-7) were collected by severing the connecting distal thread within 24 h of deposition. While attached to the slide, each plaque was rinsed for 60 sec with 18 megohm pure water (MilliPore). Following rinsing, plaques were incubated in either 5% acetic acid or filtered sea water for 30 min at room temperature with shaking at 45 rpm. Seawater treated plaques required additional washing step post treatment to remove excess salts, which interfere with the electrophoretic process. These plaques were washed 3 X @min each with transfer buffer. Following incubation, plaques were peeled from the slide with a clean single edge razor blade. Excised plaques were placed between two 0.45-micron nitrocellulose membranes (NitroPure WP4HY08250) and loaded into a semidry transfer cell (BioRad Transblot SD #1703940). 5% acetic acid conditioned plaques were electrophoresed in 0.7% acetic acid at 12 volts for 20 min. Seawater conditioned plaques were electrophoresed in 121mM Tris-glycinate pH 8.2 at 12 volts for 20 min. Although the direction of electrophoresis was initially performed in both directions, soluble components

migrated only toward the cathode. As a result, the plaque-substrate interface must face the cathode during acidic transfers and the anode during basic transfers.

***Mass spectrometry***

Proteins transferred to nitrocellulose membranes were investigated in situ by MALDI-TOF MS. For post-electroblotting transfer, the membrane was cut around the perimeter of the plaque footprint using a clean #11 scalpel. With fine nose tweezers, the plaque was removed from the membrane, which is subsequently affixed to a MSP 96 MALDI Target (Bruker) with adhesive carbon tape. 10 μL of MALDI-matrix, a saturated solution of α-cyano-4-hydroxycinnamic acid in 30% acetonitrile 1% trifluoroacetic acid, was applied to the membrane and dried in a vacuum desiccator (Nalgene). Mass spec analysis was conducted using a Microflex LRF MALDI-TOF (Bruker). Sample membranes were irradiated using a Nitrogen laser at 337 nm and a pulse length of 3ns with a repetition rate of 20 Hz. Detection occurred in linear mode between 2-20kDa at sampling rate of 1 Gs/s. Protein Calibration Standard 1 (Bruker #206355) was used as an internal calibration.

Oxidative damage to proteins was assessed by mass spectrometry. Plaques less than 48 h old were homogenized in 10mM acetic acid at a ratio of ~50mg wet weight to 1 mL acetic acid using a Dounce homogenizer. The homogenate was clarified via centrifugation at 5000xg for 5 min after which the soluble supernatant was carefully separated from the insoluble fraction. The concentration of protein was assessed via the Bradford assay kit (Thermo Fisher Pierce) and adjusted to 1 mg/mL with 10mM acetic acid. The solution was aliquoted into 5 samples and adjusted to assay conditions using the following stock buffers.

1) 10mM acetic acid
2) 10 mM acetic acid + 10mM sodium metaperiodate (Sigma Aldrich)
3) 50 mM Tris pH 8.0
4) 50 mM Tris pH 8.0 (coacervate)
5) 10 mM acetic Acid (coacervate) + 10mM sodium metaperiodate

Oxidation was tracked by acquiring spectra as time elapsed. The sample was mixed with α-cyano-4-hydroxycinnamic acid (HCCA) in 50% (v/v) aqueous acetonitrile with 0.1% trifluoroacetic acid at a ratio 1:9 and spotted onto a stainless steel MALDI target.

***Amino acid analysis of electro-transferred footprints***

Electro-transfer was performed as above except that NitroPure membranes were replaced with PVDF membranes (Immobilon IPVH00005). This change avoided nitrocellulose degradation in 6N HCl. Five blotted footprints were excised from the excess membrane and loaded into a 1mL glass ampule (Wheaton Glass, #651502) and submerged with 250 µL of constant boiling 6N HCl with 10 µL phenol. Acid hydrolysis of electro-transferred proteins was done at 110°C for 24 h under vacuum. After 24 hours the sample was removed from the vial and loaded into a LoBind microcentrifuge tube (Eppendorf, #Z666505). The hydrolysis ampule was washed with 500µL X2 of 18 megohm pure water to ensure all amino acids were transferred to the microcentrifuge tube. The now dilute HCl was removed via flash evaporation with a SpeedVac vacuum concentrator with vapor trap (Savant, Holbrook, NY). Once dried, amino acids were resuspended in 200 µL of 0.01N HCl and loaded into the automated amino acid analyzer (Hitachi High-Technologies model L-8900).

### *Polyacrylamide Gel Electrophoresis of Plaque Extracts*

Proteins can be electrokinetically extracted from single plaques for microanalysis by mass spectrometry and amino acid analysis, but these quantities are insufficient to see on a gel or to coacervate. For gels, plaques (<24 h) old were collected and pooled for bulk homogenization at a ratio of ~50mg wet weight to 1 mL of either 0.7% acetic acid pH3 or 121mM Tris-glycinate pH 8.2 to match electro-transfer conditions. The homogenate was clarified via centrifugation at 5000g for 10 min at which point the supernatant solution was carefully separated from the insoluble fraction. The pH 8.2 homogenate was then dialyzed against 0.7% acetic acid >4h at 4°C. Both homogenates were mixed 1:1 with gel loading buffer (5% Acetic acid 8M Urea) (*31*) and 10µL was loaded onto a preequilibrated 7.5% Acid-Urea gel (10 mA for 2 hours). The gel was run with 5% acetic acid serving as the tank buffer in a RioRad Mini Protean Tetra Cell at a constant current of 12 mA for 30min using a GE EPS 301 power supply. Post electrophoresis, the gel was stained with 0.1% CBB G-250 in 40% methanol 20% acetic acid for 30 min and destained with 20% methanol 10% acetic acid until the gel background became completely transparent.

## **Analyses of bulk extracted plaque proteins.**

### *Thiol and Dopa Quantification*

Because Dopa and Cysteine are important to protein redox these functionalities were independently quantified for comparison to amino acid analysis. Plaques (<48 h old) were homogenized in 10mM acetic acid at a ratio of ~50mg wet weight to 1 mL acetic acid using a Dounce homogenizer on ice. The homogenate was clarified via centrifugation at 5000xg for 10 min effectively separating the soluble supernatant from the insoluble pellet. A stock

of Ellman's Reagent (Thermo Fisher) was made 4mg/mL in dimethyl sulfoxide. Guanidine-HCl (Fisher) was dissolved in reaction buffer (RB, 0.1M HEPES, 1mM EDTA pH 8) to a final concentration of 6M. 107µL of RB was added to 30 µL guanidine and 40µL homogenate and mixed via aspiration to ensure homogeneity of the solution. 10 µL of stock Ellman's Reagent was added to the mixture and allowed to react for 15 min prior to measuring the absorbance at 412 nm (*33*). Concentration of thiols in the homogenate was calculated from a standard curve of cysteine-HCl monohydrate. The standard curve was created by make 2-fold serial dilutions of cysteine from 2mM to 0.08mM. Dopa was quantified in aliquots of the 10mM extract supernatants using an adaptation of the Arnow assay (*34*) with L-Dopa or 4-methyl catechol as calibration standards.

***X-Ray Photoelectron Spectroscopy (Sulfate Identification)***

Sulfate-mediated coacervation of mfps in plaques is not biologically relevant unless sulfate levels are elevated at the plaque interface. A two-component 5-min epoxy was mixed and deposited into a 6 x 6 mm square face mold (Electron Microscopy Sciences, Hatfield, PA). A fresh mussel plaque was excised from the mussel using a clean single edge razor and mounted with the thread down (plaque interface up) into the exposed underside of partially cured epoxy. Sulfate was detected via X-ray photoelectron spectroscopy using a Thermo Fisher ESCALAB XI spectrometer with Al Kα X–ray source. An overview spectrum was gathered from 700 to 0 eV with a 0.5 eV step size and 100 ms dwell time. A high-resolution spectrum of the sulfur K-edge was then collected from 175 to 144 eV with a 0.1 eV step size and 250ms dwell time and summed over 6 scans. Sulfate was identified using the Casa software, fitting the S $2p^{3/2}$ with a Gaussian function centered at 168.12 eV with a full width

height mean of 1.35 eV separated from $2p^{1/2}$ by 1.18 eV (169.3eV) constrained to an intensity ratio of 2:1.

***Redox assays using diphenylpicrylhydrazyl radical (DPPH)***

DPPH (redox potential = +0.77V SHE see Table S3) is a redox dye that can be used to quantify a wide variety of reducing compounds with lower redox potentials. Plaques (< 48 h old) were collected and homogenized in 10mM acetic acid at ~50mg wet weight per 1 mL acetic acid using a Dounce homogenizer. The homogenate was clarified via sedimentation at 5000xg for 5 min after which the soluble supernatant was carefully decanted from the insoluble fraction. The concentration of protein was determined by the Bradford assay and adjusted to 1 mg/mL. The redox capacity of the solution was assessed using a published DPPH assay protocol (*32*). 50µL of protein solution was added to 900 µL of assay buffer (100 mM HEPES pH 7.4). For coacervate assays, an aliquot of 1M $Na_2SO_4$ stock was added to a final concentration of 30mM to solutions containing 1 mg/mL soluble protein and mixed with assay buffer by rapid in-out pipetting. To begin the redox reaction, 50 µL of 2mM stock DPPH (Sigma Aldrich) solution (in methanol) was added to the protein containing solution. The absorbance at 517nm was monitored as a function of time. The percentage of oxidized DPPH reagent remaining as a function of time was calculated as % DPPH remaining = ($Abs_{sample,t}/Abs_{control,t}$ x 100).

***Reconstituted coacervation and labeling of plaque proteins***

Coacervation requires mg amounts of protein particularly for doing coacervate electrochemistry and redox assays with DPPH. In vitro coacervation of plaque protein

extracts was effected by sulfate addition, which Bungenberg de Jong referred to as “complex coacervation” between microanions and macrocations. Notably, two groups have investigated on the phase behavior of recombinant mfp-3 variants coacervated by microanions such as sulfate, phosphate and citrate (*9, 10*). At a protein concentration of 1mg/ml, both reported a coacervate phase boundary at 20-40 mM sulfate, which approximates the sulfate concentration in seawater. 100 mg wet weight of plaques were collected and rinsed 3X 1min with de-ionized water and then 1X with marine phosphate buffered saline (mPBS). Plaques were homogenized in 10mM acetic acid at a ratio of 100mg/1mL. The homogenate was clarified via centrifugation at 5000g for 10min. The resulting clarified homogenate was filtered with a 0.22 μm filter and adjusted to 1mg/mL protein with 10mM acetic acid as necessary. Coacervation was induced by adding stock 1M sodium sulfate to a final concentration of 30 mM. Confocal images of phase separation were collected using a Leica SP8 confocal microscope (Leica Microsystems) fitted with 63X/1.4NA oil immersion objective and hybrid detectors (HyD). Coacervates were visualized via the intrinsic fluorescence of mfp3 excited with a 405 nm laser (*7*). In a parallel experiment in coacervating mfps in which two distinct fluorophores are present, rinsed plaques were then incubated in 0.05 μM Alexa Fluor$_{555}$ $C_2$ maleimide (Thermo Fisher Scientific, Waltham, MA) in mPBS at room temp for 2 hours while rotating on a mixer. Alexa Fluor$_{555}$ $C_2$ maleimide specifically targets Cys residues which are limited to mfp6. Following incubation, plaques were rinsed 3X 1 min with 10 mL of deionized water to remove excess fluorophore. Alexa Fluor$_{555}$ stained coacervates were visualized using the white light laser tuned to 550 nm excitation.

**D. Results**

Mussel adhesive plaques (Fig. 3.2.A) consist of an open porous architecture with two length-scales of porosity (*23*). These pores appear empty by SEM (Fig. 3.2.B) but are fluid-filled in native plaques. The interfacial film is ~15 nm thick, overlaid by a continuous mottled layer ~50-100 nm thick before the regular ~100 nm porosity begins (Fig. 3.2.C). Fig. 3.2.C/D compares two interfaces from naturally deposited plaques. One was untreated before routine processing, whereas the other was equilibrated at pH3 for 30 min. Although both plaques appeared identical to the eye, much interfacial plaque structure was disrupted at pH3 vis-à-vis controls (Fig. 3.2.D). The electron dense film and much adjoining internal structure dissolved leaving a 10-20 nm porosity mesh. Perhaps this is evidence of pH-dependent phase transitions.

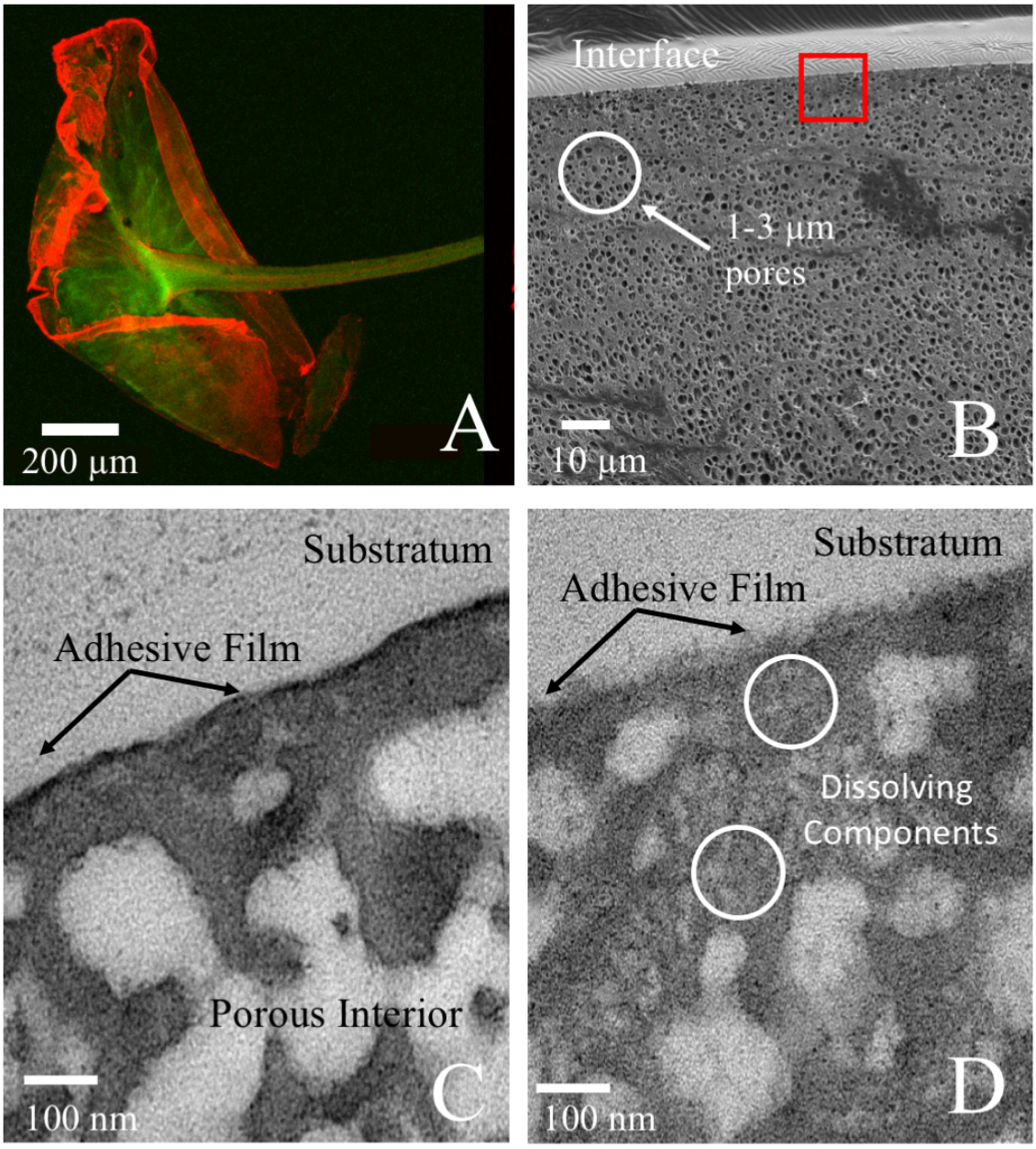


*Figure 3.2. Plaque structure at multiple length scales. A. Whole plaque with intrinsic fluorescence. B. SEM of plaque section. Area enclosed in red box is shown in panels C and D. C. TEM of untreated plaque interface; D. 5% acetic acid treated (30 min) interface shows dissolution of strut network (white circles) containing non-crosslinked protein.*

By subjecting plaque interfaces to cyclic voltammetry (CV) at pH8 and pH3, we observed a shift of +290 mV in the anodic potentials ($E_{anode}$) (Fig. 3.3.A). The relationship between redox potential and pH is linear and characteristic of the 2-electron oxidation of catechols including Dopa (*24*) (Fig. 3.3.B) and Dopa-containing mfp-3 variants (Fig. 3.3.B). The typically broader anodic peak may reflect the different local environments of Dopa in mfps (*25*). Separate analysis of plaque interfaces by XPS also detected thiols and sulfate anions (Fig. 3.3.C).

To capture and identify proteins involved in pH-induced phase transitions, we electroblotted plaques to membrane supports at different pHs (Fig. 3.3.C). Soluble proteins showed electrokinetic migration through the porous plaque mesh under an electric field. In contrast, other protein phases, e.g. coacervates, hydrogels, precipitates, stayed put. Migrating proteins were electroblotted from plaques to nitrocellulose and identified by mass spectrometry and the byssal proteome of *M. californianus* (*8)* At pH3, mfp3 and mfp6 variants predominated, particularly mfp3-1β (*m/z* 5192) and mfp3S (*m/z* 6412) variants, distinguished by the 16Da sawtooth steps associated with Dopa modifications (Fig. 3.3.D). In contrast, at pH 8, *m/z* values consistent with mfp8 and unmodified mfp3 variants were evident; mfp-6 was absent. Unmodified mfp5 was sparingly detectable (*m/z* 8910 Da) at pH 8, whereas fully hydroxylated (*m/z* 9230) mfp5 was soluble at both pHs.

We deduced unexpected insights about plaque redox from the sawtooth steps around the mfp3-1β variant peak (with *m/z* 5304 representing 7 additional hydroxylations) (Fig. 3.3.E). Step *m/z* registers provide fiducial markers of redox: each Dopa oxidized to

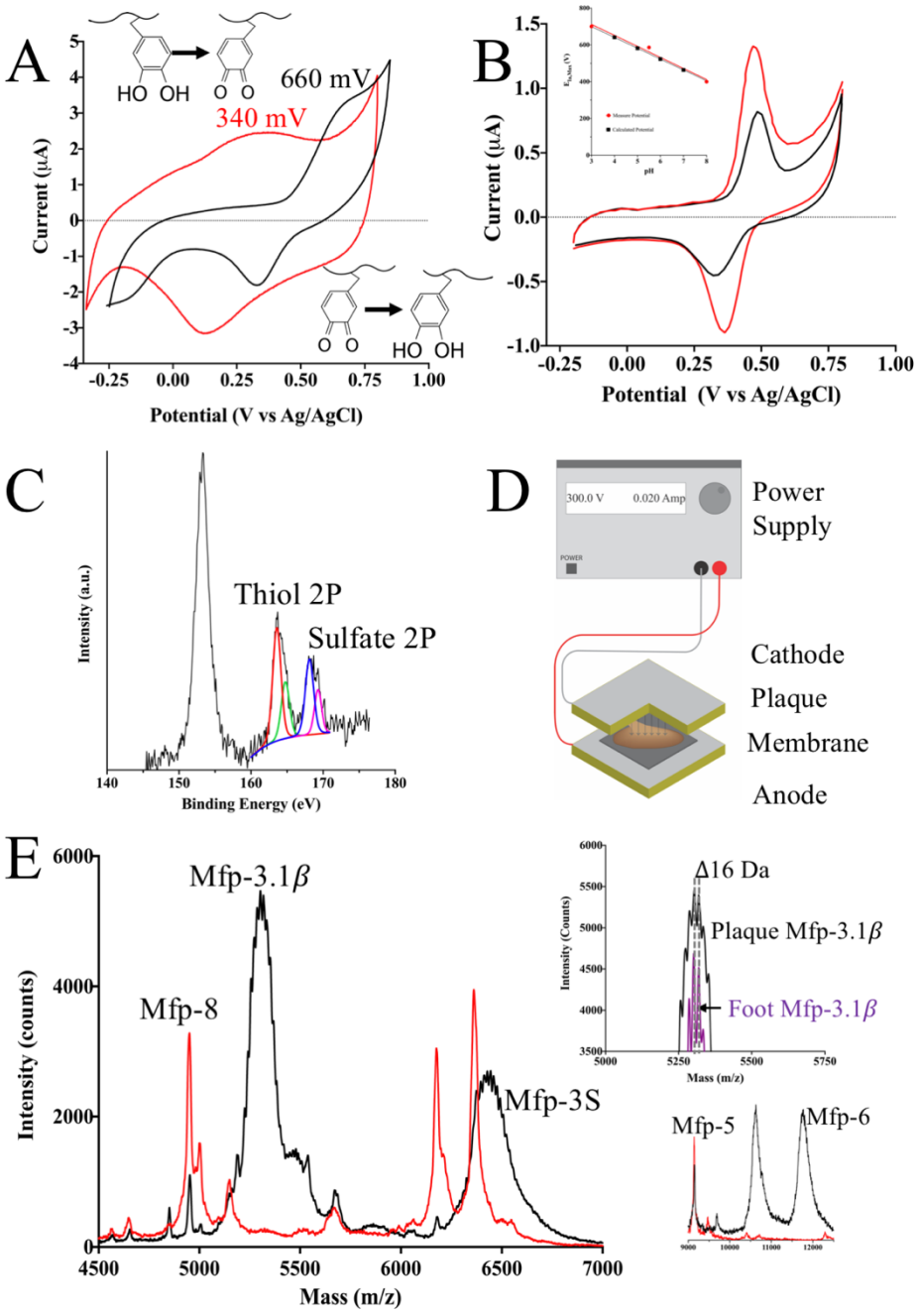


*Figure 3.3 Chemical analysis of plaque interfaces. (A) Dependence of catechol redox on pH, CV plaque, pH 3 (5% acetic acid, Black) and pH 8 (seawater, Red) showing anodic peak potentials. Glassy carbon electrode at 50 mV/s scan rate. (B) Cyclic voltammetry of purified mfp3.1β and mfp3-4 (S variant) (0.1 μM) at pH3. Gold working electrode and 100 mV/s scan rate at 20 ˚C and 1 ATM. Inset, plot of $E_a$ vs pH in plaques is linear according to the Nernst equation for reversible redox reactions that involve $H^+$ and $e^-$. Red data points were measured potentials whereas the others were predicted from the pH 3 and 8 endpoints. (C) XPS of plaque foot print on glass with sulfur speciation as thiol and sulfate peaks. (D) Electroblotting strategy used to move soluble proteins: plaque is positioned with adhesive interface facing nitrocellulose (NC) membrane and the cathode. NC was soaked in matrix, dried, and subjected to mass spectrometry. (E) Mass spectrum of electrokinetic proteins at pH 8 (red, tris glycinate) and pH 3 (black acetic acid). Top Inset,enlarged m/z of mfp3-1β showing mass register with mfp3-1β standard (purple). Bottom inset extends m/z range to 13,000.*

dopaquinone reduces the mass by 2 Da, or 20 Da for every 10 Dopaquinones. Loss of another 2 Da/Dopa or 40 Da/10 Dopas occurs upon quinone tautomer (dehydroDopa) oxidation (*26*). Thus, in the absence of intermolecular adduct formation, oxidation results in decreasing centroid *m/z*. As both 24h-old plaque and purified mfp3-1β share the same the centroid and step masses, oxidation is absent. After 14 days in seawater, however, the centroid *m/z* for plaque mfp3-1β decreased by ~7Da. In stark contrast, the centroid for mfp3S decreased by ~20 Da (Fig. 3.5.A/D), suggesting that variant mfps have differential susceptibilities to oxidation.

Detecting pH-dependent phase changes in plaques falls short of detecting dynamic liquid phases in situ, so we focused on LLPS reconstitution. Our coacervation of plaque proteins with sulfate (30mM) corroborated reports of sulfate-mediated coacervation of recombinant mfp3F (*9-10*) and was visualized by intrinsic mfp3 fluorescence (*15*) (Fig. 3.4.A). In minutes, droplet dispersions settled and spread over surfaces (Fig. 3.4.AB). Sedimented droplets exhibited the same pattern of saw-toothed mfp3 and mfp6 peaks to within 1Da of fiducial *m/z* markers but contained no detectable mfp5 or mfp8 (Fig. 3.5.A/B). Notably, mfp3S variants (*m/z* ~6200) coacervated in vitro showed evidence of oxidation after one coacervation/ solubilization cycle (Fig.3.5.A), corroborating differential variant susceptibility. Inhomogeneous droplet compositions are suggested by coacervating plaque proteins with AlexaFluor555$C_2$-labeled mfp-6 (Fig. 3.5.E/F).

Proteins bulk-extracted from plaques at pH 3 exhibited an anodic peak potential ($E_a$) of +440mV with a linear plot of current vs scan rate$^{1/2}$ indicating soluble mfps with reversible DOPA redox (Fig. 3.3.B, Figs. 3.6; ). When the same cohort of mfp's was coacervated by

sulfate, Dopa $E_a$ was +101 mV more resistant to oxidation but redox was less reversible (Fig. S5A, E).

To confirm redox insulation, we compared redox exchange by soluble and coacervated mfps with two strong oxidants, the redox dye diphenylpicrylhydrazyl radical (DPPH· $E_0'$ +0.6V vs Ag/AgCl) (*21*) and periodate ($E_0'$ +1.2V). Exchange between DPPH· and soluble plaque-derived mfps at pH 8 was detected by DPPH· bleaching (Fig. 3.4.C), whereas, sulfate-coacervated mfps resisted redox exchange for ~50 min (Figs. 3.4.C; Fig.3.5.D). Coacervated mfps also resisted redox exchange with periodate such that no change in centroid *m/z* was observed in coacervated samples at either pH3 or pH8 for >120 min (Fig. 3.4.D).

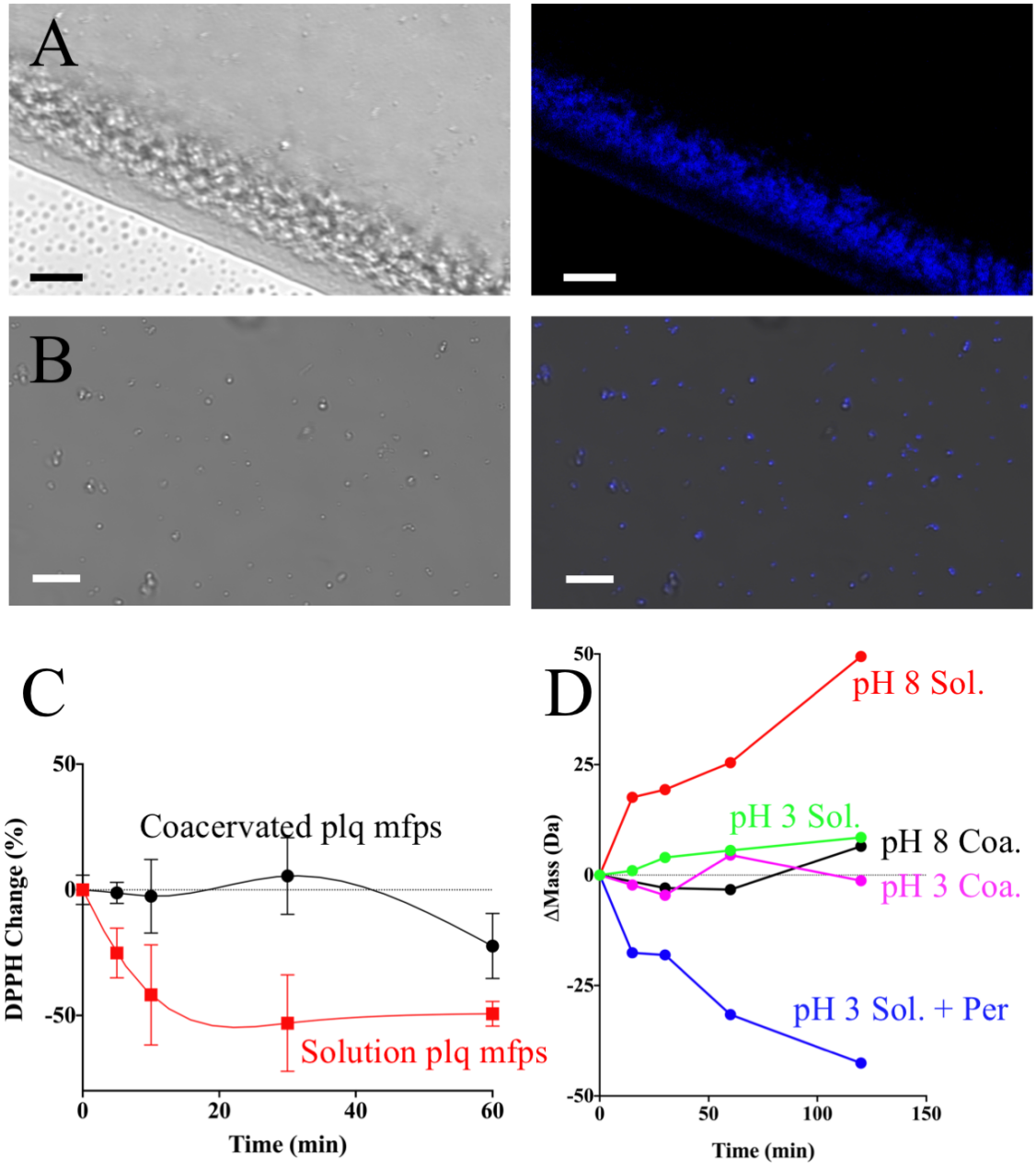


*Figure 3.4. A. Confocal images of settled (top) and suspended (bottom) coacervate protein microdroplets. Visible micrograph (left) and fluorescent image (right). B. Comparing redox exchange between 0.1 mM DPPH and plaque protein/sulfate coacervates or soluble plaque proteins. Scale bar is 5μm. Oxidized DPPH is purple ($\lambda_{max}$ 515 nm) and undergoes bleaching by reductive redox exchange with available Dopa and/or thiol groups. % change DPPH denotes [DPPH-DPPH$_2$]/DPPH x 100 or the proportion by which initial DPPH color decreases over time. D. Redox exchange between 10 mM periodate and soluble or coacervated plaque proteins at pH3 and 8. At pH 8, oxidation occurs without periodate and quinones add tris to increase in mass.*

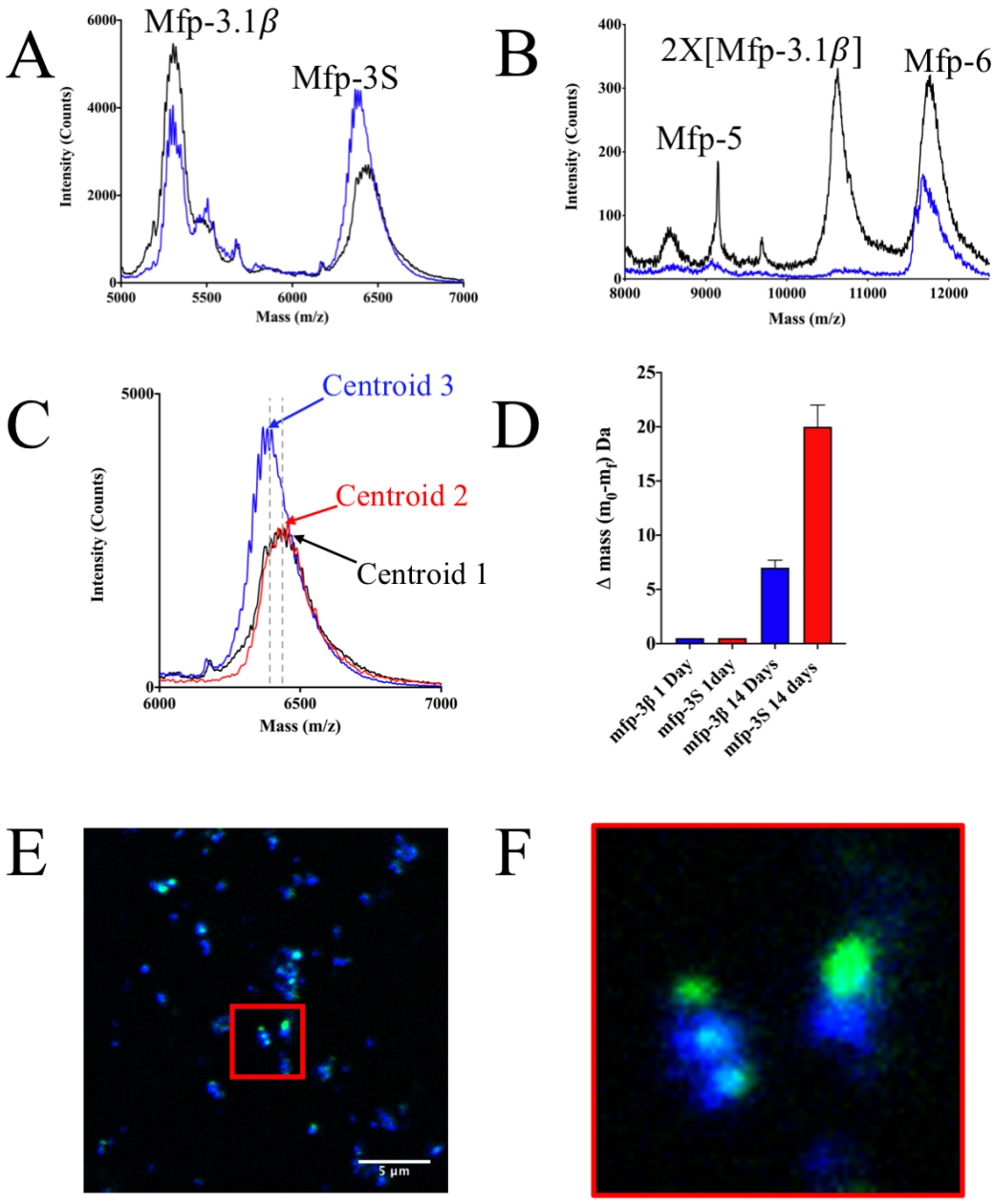


***Figure 3.5*** *Phase-dependent identity of redox active plaque proteins. A and B. Comparing protein masses extracted from plaques at pH 3 and reconstituted plaque coacervates by MALDI TOF mass spectrometry. Note that the two panels have 10-fold difference "intensity" scales. Major differences are the absence of mfp-5 and the mfp-3 dimer in the coacervates. C. Example of using shifts in the 16Da step registers as evidence of oxidation damage. m/z centroid 2 (blue trace) has migrated to lower values compared with unoxidized mfp3S purified from foot (red) and acid extracted from 1-day old plaques (black). This shift corresponds to ~48 Da and is consistent with the oxidation of 12 Dopa residues to 12 Δ-Dopaquinones. D. Comparison of oxidation damage to mfp3.1β and mfp3S in plaques collected after 1 and 14 days. Damage is measured as the magnitude of –Δm/z compared with the undamaged precursor (mean and std deviation n=3). Confocal fluorescent imaging of coacervate microdroplets reconstituted from plaque extracted proteins using 30mM sulfate. E. Intrinsic fluorescence of mfp3 (excitation 405 nm) overlaid with Cys in mfp6 thiol-labeled with Alexa fluor 555 C2 excitation was at 550 nm. F. zoom of E highlighting droplets with different mfp contents perhaps undergoing coalescence.*

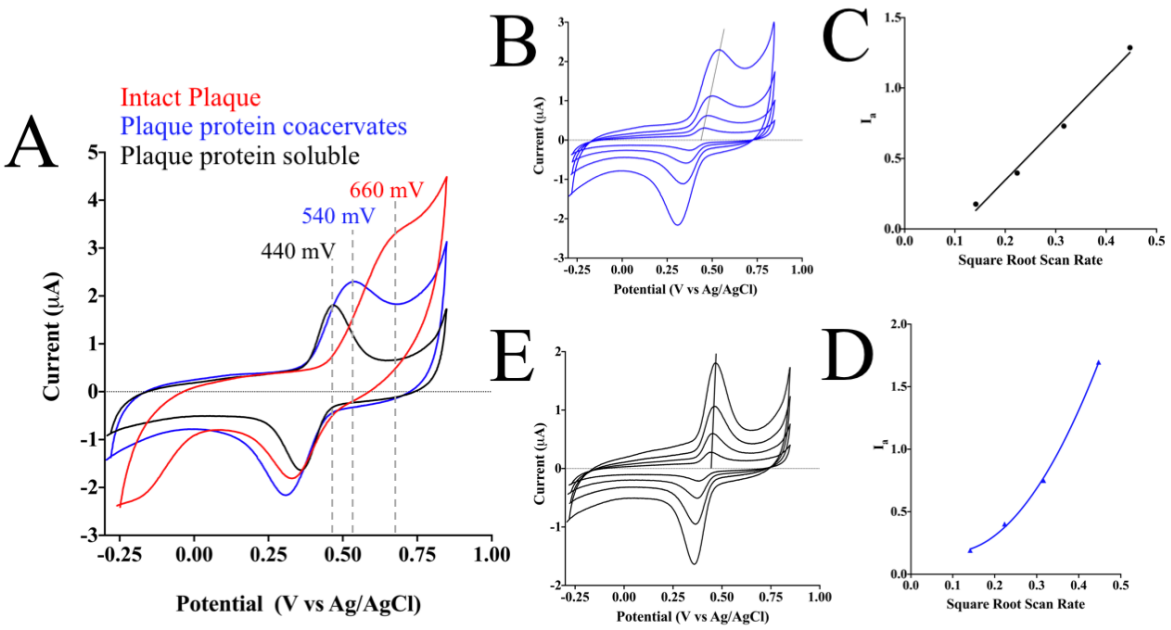


***Figure 3.6.*** *Cyclic voltammetry of pH3 plaque-derived proteins after different treatments. A) CVs of plaque-extracted proteins in solution at pH 3 (black trace); 30 mM sulfate mediated phase separation of plaque extracted proteins in dense coacervate phase (blue trace); scan of a plaque interface in situ (red trace). Oxidation potentials are indicated. B) CV of soluble plaque proteins at pH 3 and 4 different scan rates (20, 50, 100, 200 mV/s); C) correlation of peak current with square root of scan rate. $I_p$ vs (scan rate) $^{½}$ is linear, therefore redox is reversible; D) coacervated plaque proteins at pH 3 and 4 different scan rates (20, 50, 100, 200 mV/s); E) dependence of peak current and potential on scan rate. $I_p$ vs (scan rate) $^{½}$ is nonlinear.*

Mussels are masters of interfacial Dopa redox control in plaques. Success may rely on maintaining two phase-separated and redox-regulated compartments (**C**) of Dopa in the plaque: **C1** is a 15 nm-thick interfacial film of mfp-5 and mfp-8 with a high $E_{an}$; **C2** is a 10-20 nm open-pore mesh filled with coacervate droplets of mfp-3 and mfp-6 and a $E_{an}$ ~120 mV lower than **C1**. We propose the following redox interplay to maintain Dopa-dependent adhesion (Fig. 3.7.A/B): *i)* Dopa-containing interfacial mfps in **C1** regularly sustain damage by oxidation to quinone; *ii)* unable to rebind the surface, the **C1** quinone H-bonds to accessible Dopa in **C2**, and, given the significantly more positive $E_{an}$ of **C1** Dopa, undergoes redox exchange to restore Dopa for adhesion; *iii)* **C2** Mfp-3 now has Dopaquinone, which it recycles to catechol using $2e^- + 2H^+$ from two thiols in mfp-6, or by simple tautomerization to the vinylcatechol (*26*). Dopa and thiol groups in **C2** thus provide a lifeline of electrons and protons for oxidized Dopa in **C1** until the reservoir is depleted. Indeed, mfp-3 and mfp-6 droplets resemble dedicated batteries for maintaining Dopa-dependent adhesion in the film.

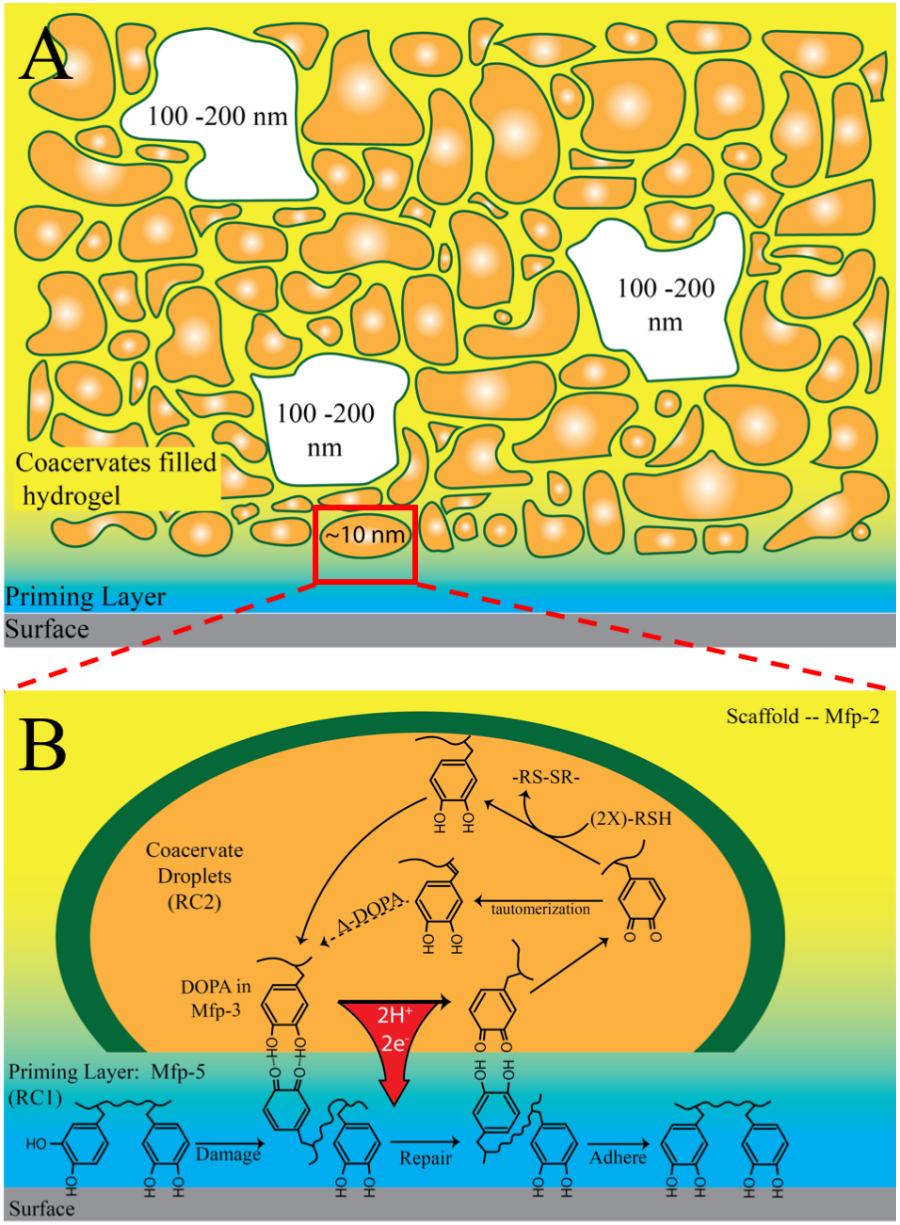


***Fig. 3.7.*** *Phase-specific Dopa and thiol redox in coacervated plaque proteins. A. Schematic plaque interface; B. Enlarged droplet with mfp3 and mfp6 variants. C1 is the film below the droplet and contains adhesive primers mfp5 and mfp8. When C1 Dopa is oxidized to Dopaquinone ($E_a$ +660 mV Ag/AgCl; Table S3), the damage is repaired with $2H^+ + 2e^-$ donated by C2 ($E_a$ +540 mV). C2 Dopaquinone is reduced back to Dopa by thiols in mfp6 ($E_a$ -200 mV), but when thiols are depleted, Dopa derivatives (Δ-Dopa) provide reducing poise. Bidentate hydroquinone-quinone interactions actuate redox exchange in many cellular pathways (29).*

## E. Conclusions

Our results reveal that mussel plaques are core-shell structures with the adhesive film as the shell and a coacervate-filled hydrogel as the core. Although hydrogels are receiving much scrutiny for engineering tough interfaces (*27*), replacement of the water with coacervates in these gels is a novel twist that merits particular scrutiny. Coacervation as a natural strategy for protecting redox-sensitive functionalities from oxidation has a profound bearing on improved translation of wet adhesion (40-41) as well as phase-specific redox in phase-separated compartments elsewhere in biology (*1, 28*). Evidently, by sequestering oxidation prone groups within fluid-filled inclusions in a porous structure like the plaque, the groups can be shielded and recruited for redox exchange with external functionalities damaged by oxidation.

## F. References


1. A.A. Hyman, C.A. Weber, F. Jülicher, Liquid-liquid phase separation in biology. *Annu. Rev. Cell. Dev. Biol.* 30, 39-58 (2014).
2. B. Vrhovski, S. Jensen, A.S. Weiss, Coacervation characteristics of recombinant human tropoelastin. *FEBS Journal* 250, 92-98 (1997).
3. H. J. Jin, D. L. Kaplan, Mechanism of silk processing in insects and spiders. *Nature* 424, 1057-61 (2003).
4. Y. P. Tan, et al., Infiltration of a chitin by protein coacervates defines the squid beak mechanical gradient. *Nature Chem Biol 11,* 489-495 (2015).
5. M. Yamanaka, Y. Ishizaki, T. Nagakawa, A. Taoka, Y. Fukumori, Purification and characterization of coacervate-forming cuticular proteins from *Papilio xuthus* pupae. *Zool. Sci.* 30, 534-542 (2013).
6. H. Zhao, C.J. Sun, R.J. Stewart, J.H. Waite, Cement proteins of the tube building polychaete *Phragmatopoma californica. J. Biol. Chem.* 280, 42938-42944 (2005).
7. W. Wei, Y. Tan, N. R. Martinez, J. Yu, J. N. Israelachvili, J.H. Waite, A mussel-derived one-component adhesive coacervate. *Acta Biomaterialia, 10, 1663-1670* (2013).
8. D. G. DeMartini, J.M. Errico, S. Sjöström, A. Fenster, J.H. Waite, A cohort of new adhesive proteins identified from transcriptomic analysis of mussel foot glands. *J. R. Soc. Interface 14, 20170151* (2017).
9. B. Yang, S. Jin, Y. Park, Y.M. Jung, H. J. Cha, Coacervation of interfacial adhesive proteins for initial adhesion to a wet surface. *Small* 14, 1803377 (2018).
10. J. Wang, T. Scheibel, Coacervation of the recombinant *Mytilus galloprovincialis* foot protein-3b. *Biomacromolecules* 19, 3612-3619 (2018).
11. S. Kim, H. Y. Yoo, J. Huang, Y. Lee, S. Park, S. Park, S. Jin, Y.M. Jung, H. B. Zeng, D.S. Hwang, Y.S. Jho, Salt triggers the simple coacervation of an underwater adhesive when cations meet aromatic π electrons in seawater. *ACS Nano* 11, 6764-6772 (2017).
12. D. S. Hwang, H. Zeng, A. Srivastava, M. Tirrell, J. N. Israelachvili, J. H. Waite, Complex coacervation of a recombinant mussel adhesive protein and hyaluronic acid - viscous and interfacial properties. *Soft Matter* 6, 3232-3236 (2010).
13. I. Kaminker, W. Wei, A.M. Schrader, Y. Talmon, M.T. Valentine, J.N. Israelachvili, J.H. Waite, S. Han, Simple peptide coacervates adapted for rapid pressure sensitive wet adhesion. *Soft Matter* 13, 9122e (2017).
14. J. H. Waite, Mussel adhesion – essential footwork. *J. Exp. Biol. 220,* 517-530 (2017).
15. J. Saiz-Poseu, J. Mancebo-Aracil, F. Nador, F. Busque, D. Ruiz-Molina, The chemistry behind catechol-based adhesion. *Angew. Chem. Int. Ed.,* 58, 696-714 (2019).
16. G.P. Maier, C.M. Bernt, A. Butler, Catechol oxidation: considerations in the design of wet adhesive materials. *Biomaterials Science* doi: 10.1039/c7bm00884h (2017).

17. N.R. Martinez Rodriguez, S. Das, Y. Kaufman, J.N. Israelachvili, J. H. Waite, Interfacial pH during mussel adhesive plaque formation. *Biofouling* 31, 221-227 (2015).

18. J. Yu, E. Danner, R. K. Ashley, J.N. Israelachvili, J. H. Waite, Mussel protein adhesion depends on interprotein thiol-mediated redox modulation. *Nature Chem. Biol.* 7, 588-590 (2011).

19. C. Zhong, T. Gurry, A.A. Cheng, J. Downey, Z. Deng, C.M. Stultz, T.K. Lu, Strong underwater adhesives made by self-assembling multiprotein nanofibres. *Nature Nanotech.* 9, 858-866 (2014).

20. L. H. N. Cooper, Oxidation-reduction potential of seawater. *J. Mar. Biol. Ass. UK*, 22, 167-176 (1937).

21. D. R. Miller, J. E. Spahn, J. H. Waite, The staying power of adhesion-associated antioxidant activity in *Mytilus californianus. J. R. Soc. Interface 12,* 20150614 (2015).

22. A. Jain, R. D. Vale, RNA Phase transitions in repeat expansion disorders. *Nature* 56, 243-247 (2018).

23. E. Filippidi, D.G. DeMartini, P. Malo de Molina, E.W. Danner, J. Kim, M.E. Helgeson, J.H. Waite, M. T. Valentine, Fine microscopic network structure of mussel (*Mytilus*) plaques. *J. R. Soc. Interface* 12, 20150827 (2015).

24. G. M. Proudfoot, I.M. Ritchie, Cyclic voltammetric study of some 4-substituted benzene-1, 2 diols. *Austral. J. Chem.* 36, 885-894 (1983).

25. W. Wei, J. Yu, C. C. Broomell, J. N. Israelachvili, J. H. Waite, Hydrophobic enhancement of Dopa mediated adhesion in a mussel foot protein. *J. Am. Chem. Soc.* 135, 377-383 (2013).

26. R. Mirshafian, W. Wei, J.N. Israelachvili, J. H. Waite, α, β-Dehydro-Dopa: a hidden participant in mussel adhesion. *Biochemistry 55,* 743-750 (2016).

27. J. Yang, R. Bai, B. Chen, Z. Suo, Hydrogel adhesion: a supramolecular synergy of chemistry, topology, and mechanics. *Adv. Func. Mat.* 1901693 (2019).

28. Y Shin, C.P. Brangwynne, Liquid phase condensation in cell physiology and disease. *Science* 491, 357 (2017).

29. J. Regeimbal, S. Gleiter, B.L. Trumpower, C. Yu, M. Diwakar, D.P. Ballou, J.C.A. Bardwell, Disulfide bond formation involves a quinhydrone-type charge transfer complex. *PNAS 100,* 13779-13784 (2003).

30. C.A. Monnier, D. DeMartini, J.H. Waite, Adaptive mussel coatings: intertidal exposure favors soft studded armors. *Nature Commun. 9: article 3424* (2018).

31. S. Panyim, R. Chalkley, High resolution acrylamide gel electrophoresis of histones. *Arch. Biochem. Biophys.* 130, 337-346 (1969).

32. S.C.T. Nicklisch, J.E. Spahn, H. Zhou, C.M. Gruian, J.H. Waite, Redox capacity of an extracellular matrix protein associated with adhesion in *Mytilus californianus. Biochemistry 55,* 2022-2030 (2016).

33. T. E. Creighton, in *Protein Structure – A Practical* Approach (ed Creighton, T.E.) 155-168 (IRL Press, Oxford, UK, 1989).

34. J. H. Waite, M.L. Tanzer, Specific colorimetric detection of o-diphenols and 3, 4-dihydroxycontaining peptides. *Anal. Biochem.* 111, 131-136 (1981).

35. H. Zhao, J.H. Waite, Linking adhesive and structural proteins in the attachment plaque of *Mytilus californianus*. *J. Biol. Chem.* 281 26150-26158 (2006).

H. Zhao, N.B. Robertson, S.A. Jewhurst, J.H. Waite, missing reference

# Chapter IV

## Conclusions, Future Directions and Closing Remarks

**Conclusions**:

The most prominent chemistry in the mussel byssus is based on the catechol moiety. Specifically, 3,4-dihydroxyphenlalanine (DOPA), a catecholic nonstandard amino acid is incorporated in a majority of mussel foot proteins (mfp) and is relied upon to participate both cohesively and adhesively. Furthermore, DOPA must perform its duties at seawater conditions (pH 8.0 ionic strength 0.7M), at which DOPA oxidation is a thermodynamically favorable process when coupled to oxygen reduction. Additionally, the byssus cannot rely on cellular support to maintain functional integrity. Despite these shortcomings, byssus functional lifespan is on the order of months.

In 2011, Yu et al first suggested that mussels incorporated antioxidants, namely mfp-6, into the byssus to protect the plaque against oxidative damage. While mfp-6 demonstrated the ability to reverse oxidative damage at pH 8 *in vitro*, the strategy was short lived. Given the propensity of DOPA to oxidize in seawater simply incorporating an antioxidant is insufficient at providing long term performance.

The dissertation work outlined above, demonstrates the mussel utilizes a system of kinetically trapped redox reservoirs to insulate redox active DOPA from the surrounding environment. More specifically, in the plaque, the mussel uses liquid-liquid phase separated compartments to house specific DOPA containing proteins. By doing so it accomplishes two primary goals.

1) It creates discrete redox compartments in which the DOPA proteins have varying redox potentials. Mfp-5, found in a gel like state at the substrate interface has DOPA with the highest redox potential. Mfp-3, contained in coacervate like droplets, has DOPA with a redox potential approximately 100mV less then mfp-5, creating a redox potential cascade. In doing so mfp-3-DOPA may reduce damaged mfp-5-DOPAqunine. Additionally, when present as LLPS material, DOPA exhibited prolonged redox lifetime compared to solution state DOPA.

2) It overcomes a stochiometric deficit experienced by mfp-6's redox capacity. While cysteine is a powerful antioxidant, the concentration of redox available thiol is approximately 25 mM which is substantially less than the more than 200mM DOPA contained in the plaque. This puts the reducing equivalents at a ~15-fold deficit. Specific compartmentalization of DOPA alleviates cysteine's responsibility as the sole antioxidant amino acid.

With respect to the thread, the mussel incorporates a region of elevated sulfur content. Results from this dissertation indicate that the sulfur is contained as reduced thiols. Hence hereinafter this region will be known as the thiol rich region (TRL). Situated between the cuticle and the core, the TRL may serve as an electron reservoir to be called upon when DOPA in the cuticle is compromised. Beyond its redox responsibilities, the TRL serves as a mechanical barrier, protecting the core from contact damage propagating from the cuticle.

In conclusion, this dissertation has demonstrated the mussel is capable of controlling redox poise in the byssus through location specific mechanisms.

**Future Directions**:

In 2006 Hasheen Lee, Norbert Scherer and Phillip Messersmith published a hallmark manuscript on DOPA's role in mussel adhesion. In 2011, the importance of antioxidants effects on DOPA adhesion was highlighted and a proposed mechanism was put forth. Now, in 2019, we have expanded on that antioxidant model. While substantial progress has been made many questions still remain. Future endeavors should focus on elucidating the following gaps in knowledge pertaining to redox chemistry in the plaque: we know DOPA selectively partitions into coacervates and these coacervates can control redox poise, we do not know what acts as the "redox gate". That is to say, what interaction drives delivery of electrons from DOPA to DOPAquinone. A few possibilities are patently evident.

1. Any DOPAquinone-DOPA interaction is sufficient to drive electron transfer.
2. It must be mfp-3 → mfp-5 interaction to drive electron transfer.
    a. Catechols at the coacervate interface come into contact with quinones at the substrate interface inducing electron transfer.
    b. Phosphate groups on mfp-5 interact with basic residues in mfp-3 pulling the quinone into the coacervate leading to electron transfer.

Independent of the redox gate scenario, the mechanism of electron transfer should be investigated. One plausible configuration is the formation of a quinhydrone like structure in which a charge transfer complex is formed between aromatic stacks and stabilized via hydrogen bonding. Additionally, the effect of local protein sequence on DOPA's redox potential should be thoroughly explored.

With respect to the thread, a cohort of cysteine rich proteins, namely mfp-16 -17 -18 and -19 were identified in the transcriptome. Mfp-17 was positively identified at the protein

level in the collagen granules purified from the foot, but localization in the mature thread is currently lacking. Future experiments should focus on localization of the putative thiol rich proteins. MALDI-mapping may provide a viable platform for localization. Additionally, given cysteines extreme reactivity, efforts should be made to identify covalent crosslinks. Given the proximity of DOPA in the cuticle to thiol in the TRL, 5-cysteinylDOPA is a possible candidate.

Additionally, another crosslinking possibility, all be it a far-fetched exotic idea, is an isopeptide bond. Mfp-1 in the cuticle contains elevated levels of lysine, a prime candidate for isopeptide linkages. Isopeptide bond formation is often catalyzed by transglutaminase, an enzyme containing a cys-his-asp catalytic triad, and in some instances utilizes calcium as a cofactor. While Kim et al. successfully demonstrated lysine's involvement in cation pi-interactions in the cuticle, isopeptide bonds could potentially serve to bond the cuticle to the TRL/core. Interestingly, all of the components necessary for isopeptide bond formation are found in elevated levels directly adjacent to the TRL. Anti-isopeptide antibodies are commercially available thus could serve as a "low hanging fruit" opportunity experiment.

**Closing Remarks**:

Mussel byssus projects have spawned many successful careers around the globe, with Dr. Waite being a central figure in each one. Herb's success is largely due to his unwavering dedication to his principles and moral compass. Accompanying his dedication is a level of humility rarely displayed by others. This combination of attributes has allowed Herb to produce meaningful science guided principally by curiosity and substantive

questions asking. As a result, Herb's work has been increasingly used as inspiration for biologists and engineers alike, evident by the following.

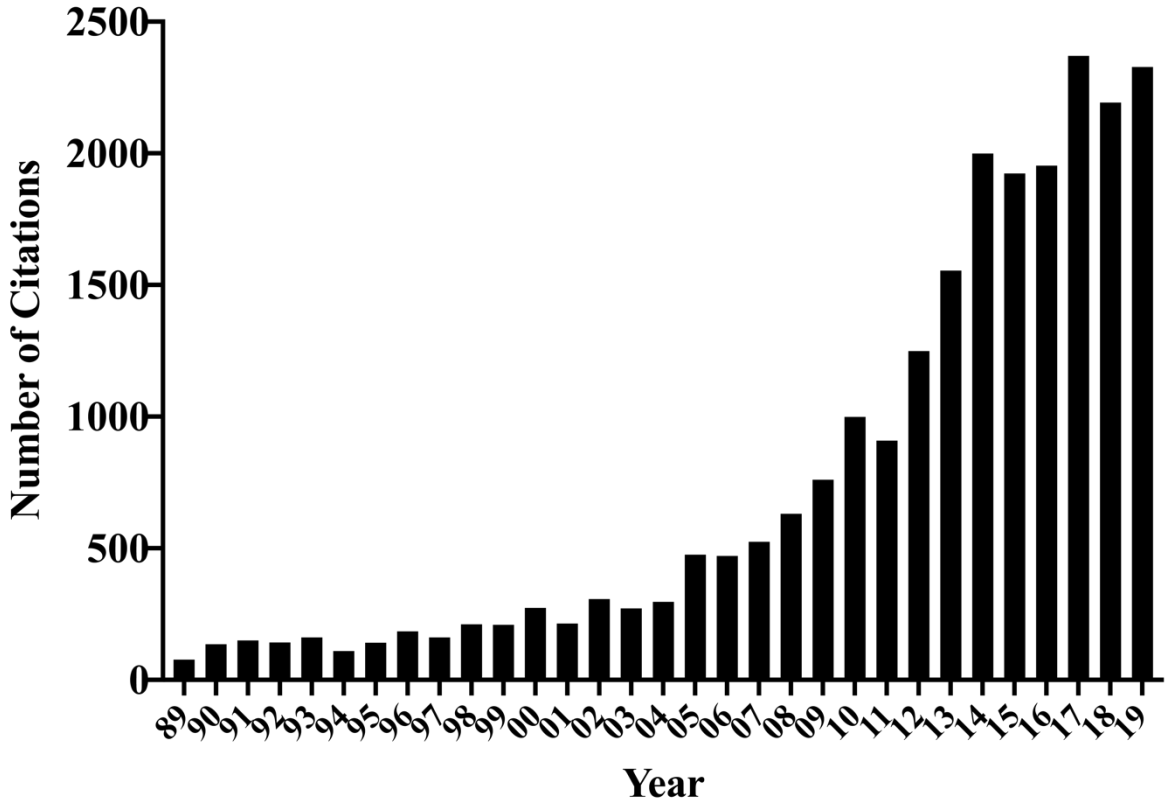


Anyone who has spent an extended period of time with Herb knows he has many "Herbisms" but perhaps the most penetrating and long-lasting ism; "Be a diver not a surfer". Translation; in order to do something truly transformative and impactful, you must go beyond the superficial and dive deep into the meaning of the

question. This is becoming increasingly difficult as funding agencies look toward application-based science. Despite this, as Herb trainees we have a responsibility to continue to push ‘basic’ research projects and to promote collaborations between fundamentalists and “engineers”. To close, I will leave you with the following quote from Herb.

“A significant lesson emerging from research on mussel adhesion that is widely applicable to other organisms is that there is no substitute for penetrating biological exploration at many length and time scales. Indeed, this exploration is as essential for good translation as it is for discovery. As reviewers and funding agencies place more and more emphasis on translation for its own sake we should stand together to insist that a retreat from the biology is counter-productive and may even be a misuse of taxpayer money. Translations driven by superficial impressions or fantasies about biology will not stand the test of time because they have missed the point.”

- J. Herbert Waite (2019)